CHAPTER X

IMMERSED BOUNDARY METHODS FOR THERMOFLUIDS PROBLEMS

Rajat Mittal[1,*] & Rajneesh Bhardwaj[2]

[1] Department of Mechanical Engineering, Johns Hopkins University, Baltimore, MD, 21218 USA

[2] Department of Mechanical Engineering, Indian Institute of Technology Bombay, Mumbai 400076, India

[*]Address all correspondence to: Rajat Mittal, E-mail: mittal@jhu.edu

We review the progress in the development and application of immersed boundary methods to thermofluids problems, achieved in the last three decades. The implementation of different heat transfer boundary conditions, ranging from Dirichlet, Neumann and Robin, to conjugate heat transfer are discussed for continuous as well as discrete forcing immersed boundary methods. We review several key studies that developed and employed IB methods with stationary boundaries for a variety of heat transfer scenarios such as forced convection, natural or mixed convection, radiation, and combustion. The computational challenges associated with and approaches employed for thermofluid problems with moving boundaries are discussed in detail. These include problems with rigid bodies that move under the influence of fluid dynamic forces, as well as flow-induced deformation of compliant bodies. We conclude the article by discussing briefly the implementation of immersed boundary methods in two emerging areas: bioheat transfer and very high-speed compressible flows.

KEY WORDS: *Immersed boundary method, Moving boundary problems, thermofluid dynamics, Heat transfer enhancement, Bioheat transfer, Supersonic and hypersonic flows*

1. INTRODUCTION

The transfer of heat from a fluid or a structure to its surroundings in most situations involves boundaries that are topologically complex. Examples include heat sinks[1], heat exchangers[2], high density electronics[3], metal foams[1], internal combustion engines[4] and hypersonic vehicles[5] (Fig. 1, left column). In many applications, the boundary might also be moving and/or deforming, such as in heat-exchangers that exploit fluid-structure interaction[6,7] or active materials[8,9]. Heat exchange with moving boundaries is also encountered in materials processing[10], high-velocity impact problems[11], and in multiphase flows[12].

ISSN: 1049–0787; ISBN: xxx–x–xxxxx–xxx–x/xx/$35.00 + $00.00

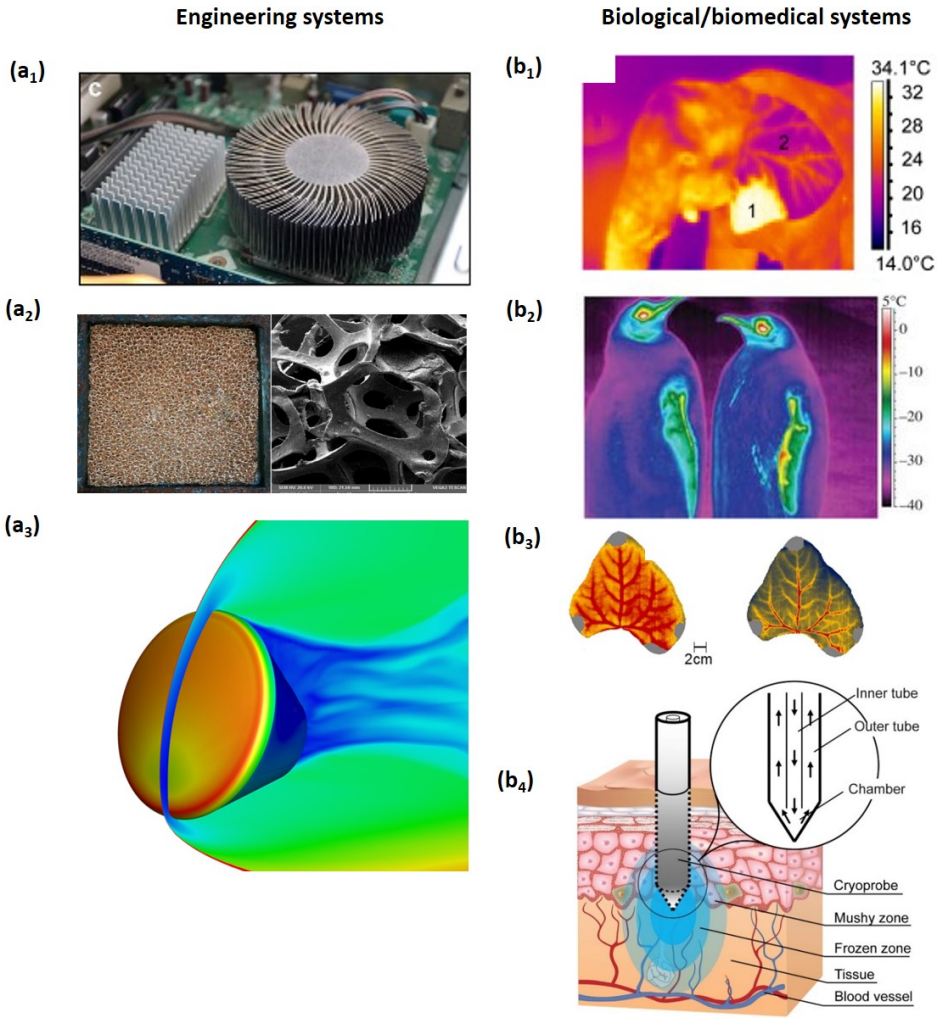

FIG. 1: A multitude of applications involving thermofluids problems in engineering, biological and biomedical systems. (a_1) Radial aluminum heat sink for enhancing heat dissipation of an electronic chip[13]. (a_2) Copper foam-based heat sink[1]. (a_3) Isotherms on the surface of Orion spacecraft and Mach number contours on the symmetry plane[5]. (b_1) Infrared thermograph of left ear of an African elephant, observed indoors at a mean ambient temperature of 19.5°C[14]. (b_2) Infrared thermograph of two emperor penguins, showing temperature variation on head and flippers in an ambient temperature of -21.8°C[15]. (b_3) Variation of temperature on a leaf of bean plant after giving a heat pulse, with wind speed of zero (left) and 0.4 m/s (right). (b_3) A schematic of tissue with an inserted cryoprobe during cryosurgery[16]. All figures have been reproduced with permissions from respective copyright holders.

Examples of fluid-structure-thermal interaction also abound in biology, and usually involve thermoregulation in animals, birds, marine animals, insects and plants (Fig. 1, right

column). For example, elephants thermoregulate their bodies via the flapping of their large ears[14]. Bees achieve thermoregulation of their nest by coordinated wing flapping inside their hive[17]. Plant leaves exchange heat and mass with their surroundings in a complex manner that involves ambient wind currents[18]. In biomedical engineering, radio frequency ablation or cryosurgery involves heat transfer in the complex vascular system of the human body and diseased tissue[16].

Over the last 50 years, computational thermofluid modeling (CTFM) has emerged as a powerful modality not just for the analysis of such thermofluid problems, but also for the design, testing and optimization of associated devices/systems. While, earlier efforts in CTFM were limited to relatively simple configurations with stationary boundaries, the state-of-the-art in this arena is rapidly moving towards configurations such as those described above that involve more complex physical as well as thermal interactions between the fluid and the structure. The fluid flow and heat transfer in these problems are inherently unsteady and strongly coupled with the structure (or the moving boundary), which itself might exhibit geometric and material non-linearities. Accurate and stable CTFD simulations of these problems can pose a significant challenge.

Immersed boundary (referred to as IB, hereafter) methods, where simulations are conducted on stationary, boundary-non-conforming Cartesian grids, are well-suited to handle the problems/configurations described above. The use of Cartesian makes it easy to solve problems with topologically complex boundaries. For instance, generation of a body-conformal grid for solving conjugate heat transfer in a metal foam is quite tedious but the problem can be tackled quite easily using a Cartesian grid based immersed boundary method[19]. For problems with moving boundaries, the use of IB method also eliminates the added complexity associated with remeshing, which usually accompanies other body-conformal grid methods (e.g. Arbitrary Lagrangian-Eulerian method (ALE) method[20]). In the past two decades, there has been a rapid growth in the development as well as the use of IB methods in thermofluids problems and the current article focuses on reviewing this progress, as well describing some future trends.

1.1 Scope of the present review

Several previous reviews in the last two decades have covered a variety of aspects of these methods; these include reviews by Peskin[21], Mittal and Iaccarino[22], Iaccarino and Verzicco[23], which focused on describing different formulations of the IB methods and associated applications. IB methods have also been successfully developed and applied in biomedical and biological flows which often involve fluid-structure interaction (FSI) and large-scale flow-induced deformation (FID). The FSI and FID aspects of IB methods have been reviewed by Sotiropoulos and Yang[24], and Griffith and Patankar[25] in greater details. Some recent reviews[26–28] have also described the progress in this arena. In this current review we focus on new developments and applications of the IB methods with a particular focus on thermofluids problems.

In this article, we first review IB methods for a variety of heat transfer scenarios in thermofluids problems where the boundary is stationary. The implementation strategies

within the IB framework for different heat transfer boundary conditions, including those for conjugate heat transfer, are discussed. Following this, the application of IB methods to thermofluids problems that exhibit large-scale flow-induced boundary/structure deformation, are reviewed. We conclude this article by reviewing the IB applications in two emerging areas in thermofluids: bioheat transfer and high-speed flows. This review does not cover IB treatment of the following situations: moving fluid-fluid interface (i.e., multiphase flows), mass transfer across fluid-fluid interface and phase change across fluid-fluid or fluid-solid interface. Some of the IB implementations in these topics have been reviewed by Xiao et al.[29].

1.2 Overview and classification of IB methods

The term "immersed boundary method" was used first in the context of the methods developed by Peskin nearly four decades ago[30–33]. In this original implementation of the IB methods, the fluid flow was computed on a fixed Cartesian grid, and the solid boundary was modeled using a dense mesh of massless elastic fibers. The fibers were assumed to move with the local flow and exert a localized force on the fluid. This two-way interaction was modeled by a set of localized forces and this force distribution was "regularized" for implementation on a discrete mesh. Since the proposition of Peskin's method, there has been tremendous growth, evolution and diversification in IB methods. A key contribution in this arena was the feedback control based forcing that was introduced by Goldstein et. al.[34] to apply the IB method to solid walls.

As suggested by Mittal and Iaccarino[22], IB methods may be classified in to two broad categories: continuous forcing[32,32,34–41] and discrete forcing methods. The former approach introduces a localized source term in the continuous form of the momentum equations to model the interaction between the fluid and the immersed boundary. Subsequent discretization of this augmented momentum equation requires the regularization of this localized source term resulting in a "diffuse" interface. In the latter approach, the governing equations are first discretized on a Cartesian grid without accounting for the IB. Subsequently, the discretization is adjusted near the IB to incorporate the boundary conditions on the IB[22]. The discrete forcing approach allows for a "sharp" representation of the IB such as in studies by Ye et al.[42], Udaykumar et al.[43] and Mittal et al.[44] and others. While the continuous-forcing approach is easy-to-implement and computationally inexpensive as compared to discrete forcing, the diffuse interface treatment in the continuous-forcing approach can limit their application to relatively low Reynolds numbers. The discrete forcing has been further divided into sub-categories, namely, indirect boundary condition imposition[45–47] and direct boundary condition imposition[42–44,48–54]. IB methods have been implemented most commonly in conjunction with finite-difference methods but also with finite-volume[42,43,45,49] as well as finite-element formulations[37,41]. One issue with all IB approaches is that the grid size generally grows faster with Reynolds number than for body-conformal grid methods[22] and this can be only be addressed by employing local-grid refinement techniques[55–58].

1.3 Early developments of IB methods for thermofluids problems

One of the earliest implementations of IB methods to thermofluids problem was by Udaykumar and co-workers[49,50]. In these studies, a mixed Eulerian-Lagrangian technique (ELAFINT: Eulerian-Lagrangian algorithm for interface tracking) finite-volume based solver was proposed for topologically complex boundaries and moving fluid-fluid interface. In addition, this algorithm for phase change at the fluid-fluid interface modeled via Stefan condition. The flow computations were performed on a fixed Cartesian grid while the fluid-fluid interface was tracked using Lagrangian marker particles[49]. The boundary condition at the IB was imposed within the finite-volume framework using a cut-cell technique (Fig. 2 (a)). With the cut-cell technique, the shape of the cells near the IB is modified locally to conform to the boundary (Fig. 2(a)) and this allows for a strictly conservative discrete formulation. The fidelity of the solver was demonstrated using several test cases including natural convection in a closed cavity (Fig. 2 (b, c)) and the deformation of a viscous droplet.

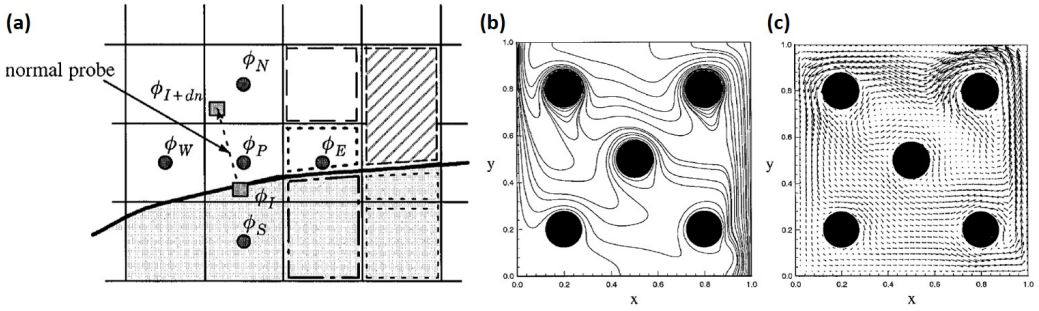

FIG. 2: One of the earliest implementation of cut-cell IB method in thermofluids[50]. (a) The cells near to IB are reshaped such that they fit locally the IB, resulting in flux conservation. A normal probe, as shown in the figure, was used to compute the gradients at the interface. (b, c) Simulated natural convection in a cavity. Pr = 1, Ra =10^6 on a 121×121 grid, showing computed isotherms (b) and velocity vectors (c) (reprinted with permission from Elsevier, copyright 1996[50]).

One of the issues in cut-cell methods is that the volume of a cut-cell could become very small, leading to numerical stability issues. Ye et al.[42] proposed a systematic cell-merging approach to alleviate this problem. While cut-cell type methods provide high accuracy and discrete conservation, they are quite complex to implement for three-dimensional problems since cut-cells of a wide variety of topologies can appear[59,60]. The treatment of *freshly cleared* cells, which are inside the solid at a given time-step and appear in to the fluid domain at the next time-step is an issue that appears in many discrete forcing methods and this issue was addressed for cut-cell type methods by Ye. et al[42] and Udaykumar et al.[43]. The implementation of fluid-fluid interface undergoing phase change was also reported[51,61,62]. A finite-difference based formulation was further developed using the sharp-interface treatment of solid boundary[63] and was applied to diffusion, convection–diffusion, and solidification problems. Some of these developments were summarized in

a review paper by Shyy et al.[64]. Later, Francois and Shyy[65,66] employed the IB method to compute the droplet dynamics on a solid substrate, including heat transfer between the droplet and the substrate.

2. STATIONARY BOUNDARY PROBLEMS

2.1 Governing equations and boundary conditions

The governing equations for flow and heat transfer in an unsteady, viscous flow are:

$$\frac{\partial \rho}{\partial t} + \frac{\partial (\rho u_j)}{\partial x_j} = 0 \tag{1}$$

$$\frac{\partial (\rho u_i)}{\partial t} + \frac{\partial (\rho u_i u_j)}{\partial x_j} = -\frac{\partial p}{\partial x_i} + \frac{\partial}{\partial x_j}\left(\mu \frac{\partial u_i}{\partial x_j}\right) \tag{2}$$

$$\frac{\partial (\rho C_p T)}{\partial t} + \frac{\partial (\rho C_p u_j T)}{\partial x_j} = \frac{\partial}{\partial x_j}\left(k \frac{\partial T}{\partial x_j}\right) \tag{3}$$

for i, j=1,2,3, where u, x, ρ, T, t, p, denote velocity, spatial coordinate, density, temperature, time and pressure, respectively. Furthermore, μ, C_p and k are the dynamic viscosity, specific heat and thermal conductivity [$\mathrm{Wm^{-1}K^{-1}}$] of the fluid, respectively, and these fluid properties may, in general, be dependent on the temperature. The Boussinesq approximation is often used to model natural convection (buoyancy-driven flows) in situations where the density differences are small[67]. Within this model, the flow is modeled as an incompressible fluid with constant density but with a buoyancy force term $g\beta(T - T_\infty)$ added to the vertical momentum equation[67], where g, β and T_∞ are gravitational acceleration, volume expansion coefficient of the fluid at constant pressure and ambient fluid temperature, respectively.

The key element in IB methods is the application of the boundary condition and it is therefore useful to enumerate the typical boundary conditions that appear for the temperature field in thermofluids problems. These extend from the simplest isothermal boundary condition (Eq. 4) to heat flux and radiative conditions[67,68], described below:

$$T = T_w \text{ on the wall} \tag{4}$$

where T_w denotes the wall temperature. A prescribed heat flux $\dot{q}_w$ [$\mathrm{Wm^{-2}}$] is expressed as a Neumann type boundary condition as follows,

$$-k\left(\hat{n}.\vec{\nabla}T\right) = \dot{q}_w \text{ on the wall} \tag{5}$$

where $\hat{n}$ is unit normal vector on the boundary. For an insulated or adiabatic surface, $\dot{q}_w$ = 0. The heat convection boundary condition is expressed as a Robin type boundary

condition as follows:

$$-k\left(\hat{n}.\vec{\nabla}T\right) = h\left(T - T_\infty\right) \tag{6}$$

where h and T_∞ are heat transfer coefficient [$\mathrm{Wm^{-2}K^{-1}}$] and ambient fluid temperature, respectively. A radiative boundary condition is a non-linear condition that is expressed as follows[68]:

$$-k\left(\hat{n}.\vec{\nabla}T\right) = \epsilon\sigma\left(T^4 - T_\infty^4\right) \tag{7}$$

where ϵ and σ are surface emissivity and Stefan-Boltzmann constant (5.670×10^{-8} $\mathrm{Wm^{-2}K^{-4}}$), respectively.

In applications involving conjugate heat transfer, the heat transfer within the solid/structure has to be modeled simultaneously via the solution of an appropriate heat conduction equation and the boundary conditions at the fluid-solid interface adjusted to account for this coupling. For the case of perfect thermal contact at the solid boundary, the temperature as well as the heat flux are continuous across the fluid-solid boundary and these conditions are expressed simply as follows,

$$T|_{\text{fluid}} = T|_{\text{solid}} \tag{8}$$

and

$$-k\left(\hat{n}.\vec{\nabla}T\right)|_{\text{fluid}} = -k\left(\hat{n}.\vec{\nabla}T\right)|_{\text{solid}} \tag{9}$$

2.2 IB Implementations of Thermal Boundary Conditions

Both continuous-forcing and discrete-forcing IB formulation have been employed to apply the boundary conditions described in Sec. 2.1. These developments are briefly summarized below.

2.2.1 Continuous forcing

In Peskin's method, massless points connected by elastic fibers represent IB and these points move with local fluid velocity and are tracked in Lagrangian framework. A forcing term is added in the momentum equation to impose the velocity boundary condition on the surface. This idea is extended to the impose a temperature boundary condition by adding a heat source/sink $q(\vec{x},t)$ [$\mathrm{Wm^{-3}}$] to the energy equation[29,69–75],

$$\frac{\partial\left(\rho C_p T\right)}{\partial t} + \frac{\partial\left(\rho C_p u_j T\right)}{\partial x_j} = \frac{\partial}{\partial x_j}\left(k\frac{\partial T}{\partial x_j}\right) + q \tag{10}$$

The heat source term is considered to be localized at the immersed boundary surface using a Delta function as follows:

$$q(\vec{x},t) = \int_\Gamma Q(\vec{X},t)\delta(\vec{x}-\vec{X})ds \tag{11}$$

where Γ represents IB, $\vec{x}$ is Eulerian coordinate, $\vec{X}$ is Lagrangian coordinate on the IB, Q is heat flux [Wm^{-2}] on the IB and δ is Dirac delta function. Following the original idea of Peskin, the discrete form of the localized source term Eq. 11 is expressed as follows,

$$q(\vec{x}_{i,j}, t) = \sum_{k=1}^{N} Q_k(t)\delta_h(\vec{x}_{i,j} - \vec{X_k})\Delta s_k \tag{12}$$

where (i, j) represent Eulerian grid point indices, $k = 1, N$ are the indices of the Lagrangian points on the IB and δ_h is a discrete Delta function. X_k is the coordinate of k^{th} Lagrangian point, Δs_k is the distance between two adjacent Lagrangian points. The temperature at the Lagrangian points is also interpolated using the temperature field at the surrounding Eulerain grid points, by the following expression:

$$T_k = \sum_i \sum_j T_{i,j}\delta_h(\vec{x}_{i,j} - \vec{X_k})h^2 \tag{13}$$

where h is the grid spacing of the Eulerian grid. δ_h serves as a kernel in transferring data between Lagrangian and Eulerian points[29] and is a smoother distribution function (Fig. 3(a)). As proposed by Peskin and co-workers[21,76], in 2D coordinates, δ_h is defined as follows:

$$\delta_h = \frac{1}{h^2}\phi(\frac{x}{h})\phi(\frac{y}{h}), \tag{14}$$

and a 4-point delta function ϕ is defined as follows[21]:

$$\phi = \begin{cases} \frac{1}{8}(3 - 2|r| + \sqrt{1 + 4|r| - 4r^2}) & \text{if } 0 \leq |r| \leq 1 \\ \frac{1}{8}(5 - 2|r| + \sqrt{-7 + 12|r| - 4r^2}) & \text{if } 1 \leq |r| \leq 2 \\ 0 & \text{otherwise} \end{cases} \tag{15}$$

The discrete delta function (Eq. 14 - 15) was employed by several previous studies[69–72,77,78] in the development of continuous forcing IB methods. Earlier studies also used other forms of distribution function. For example, Zhang et al.[79] used bilinear interpolation, proposed by Saiki and Biringen[80] for their continuous forcing IB method developed for forced convection. A comparison of different distribution functions used in several studies was shown by Mittal and Iaccarino[22].

The key to the IB method is to determine the heat source distribution $q(\vec{x}, t)$ such that it enables the satisfaction of a thermal boundary condition (fixed temperature or heat flux, etc.) on the immersed surface. This is done as follows[70–72]: An intermediate temperature field T^* is first computed by time-advancing Eq. 10 without consideration of the thermal boundary condition on the immersed boundary[70–72], i.e. without the heat source term q. The corrector step employs the following time advancement that incorporates the heat

source associated with the IB as follows:

$$\rho^* C_p^* \frac{T^{n+1} - T^*}{\Delta t} = q^{n+1} \tag{16}$$

where we assume here that ρ and C_p are unchanged during this corrector step. In the case of a Dirichlet boundary condition for temperature, the temperature at the k^{th} Lagrangian point on the wall is expressed as follows,

$$T_k^{n+1}|_{\text{wall}} = \sum_i \sum_j T_{i,j}^{n+1} \delta_h(\vec{x}_{i,j} - \vec{X_k}) h^2 \tag{17}$$

Substituting $T_{i,j}^{n+1}$ from Eq. 16 into Eq. 17, the following expression for the wall temperature is obtained:

$$T_k^{n+1}|_{\text{wall}} = \sum_i \sum_j T_{i,j}^* \delta_h(\vec{x}_{i,j} - \vec{X_k}) h^2 + \sum_i \sum_j q_{i,j}^{n+1} \frac{\Delta t}{\rho^* C_p^*} \delta_h(\vec{x}_{i,j} - \vec{X_k}) h^2, \tag{18}$$

Using the relationship in Eq. 12, the above expression for the temperature at the k^{th} Lagrangian point can be rewritten as[70–73,79]:

$$\begin{aligned} T_k^{n+1}|_{\text{wall}} = & \sum_i \sum_j T_{i,j}^* \delta_h(\vec{x}_{i,j} - \vec{X_k}) h^2 \\ & + \sum_i \sum_j \sum_m Q_m^{n+1} \frac{\Delta t}{\rho^* C_p^*} \delta_h(\vec{x}_{i,j} - \vec{X_m}) \Delta s_m \delta_h(\vec{x}_{i,j} - \vec{X_k}) h^2 \end{aligned} \tag{19}$$

where m spans all the Lagrangian points. Eq. 19 is written as a system of linear equations for all Lagrangian points and is solved for the unknown vector Q^{n+1}. Next, q^{n+1} is computed via the interpolation given in Eq. 12 and the corrected temperature field T^{n+1} computed from Eq. 16. Thus, the heat source/sink is implicitly computed such that the Lagrangian temperature at the IB interpolated from the Eulerian temperature field ($T(\vec{x}, t)$), equals to the prescribed IB temperature[70,73].

In order to implement a Neumann-type boundary condition, an additional layer of "virtual" points are defined at a distance of one grid spacing, h outside the IB[72,79]. The number of virtual points are kept the same as the number of Lagrangian points and are aligned in direction normal to the IB[72,79]. The prescribed heat flux on the IB is expressed as follows,

$$\dot{q}_w = -k \frac{dT}{dn} = -k \frac{T_k|_{\text{VB}} - T_k|_{\text{wall}}}{h} \tag{20}$$

where VB implies virtual boundary. $T_k|_{\text{VB}}$ is computed using interpolation in Eq. 13 and

the wall temperature $T_k|_{\text{wall}}$ is given by,

$$T_k^{n+1}|_{\text{wall}} = \frac{\dot{q}_w h}{k} + T_k^{n+1}|_{\text{VB}} \tag{21}$$

Using $T_k^{n+1}|_{\text{wall}}$ in Eq. 19, the corrected temperature field T^{n+1} can be obtained, as described earlier for the case of Dirichlet boundary condition.

Several previous studies[69–75,79,81,82] reported the implementation of heat transfer boundary conditions in continuous forcing IB methods in Peskin's method or its variants for Dirichlet and/or Neumann temperature boundary conditions. For conjugate heat transfer boundary conditions, Kumar and Natrajan[83] developed a diffuse-interface IB method. They solved energy equation in both fluid and solid domain, which corresponds to convective-diffusive and diffusive equation, respectively, for different thermal diffusivities in both domains. A similar implementation for the conjugate heat transfer boundary conditions was reported by Favre et al.[84]

2.2.2 Discrete forcing

Fadlun et al.[47] developed one of the early discrete forcing methods to impose a Dirichlet boundary condition for a passive scalar. Kim and Choi[85] proposed an extension of Fadlun's method for both Dirichlet and Neumann boundary condition for temperature. Several studies of thermofluids problems have developed and employed methods based on the sharp interface ghost-cell method of Mittal et al.[44] for enforcing the heat transfer boundary conditions in their IB formulations[86–89], and we describe this formulation in detail here for Dirichlet, Neumann, Robin and conjugate heat transfer boundary conditions (Eqs. 4 - 9).

These thermal boundary conditions can be applied similar to the implementation of boundary conditions for momentum and pressure, as described by Mittal et al.[44]. In this scheme, the different cell types are identified in the computational domain, as shown in Fig. 3(b). First, ghost cells (referred to as GC, hereafter) are identified which are inside the solid domain and have at least one neighbor cell in the fluid domain. The value at the ghost-cell (GC) is computed so that the boundary conditions are enforced at the solid boundary or IB. A normal is defined from the GC which meets at the "boundary intercept" (BI) point. The normal is extended beyond the BI to the "image point" (IP) in the fluid domain. The IP is usually selected so that the BI at the midpoint of the line segment joining IP and GC (Fig. 3(b)).

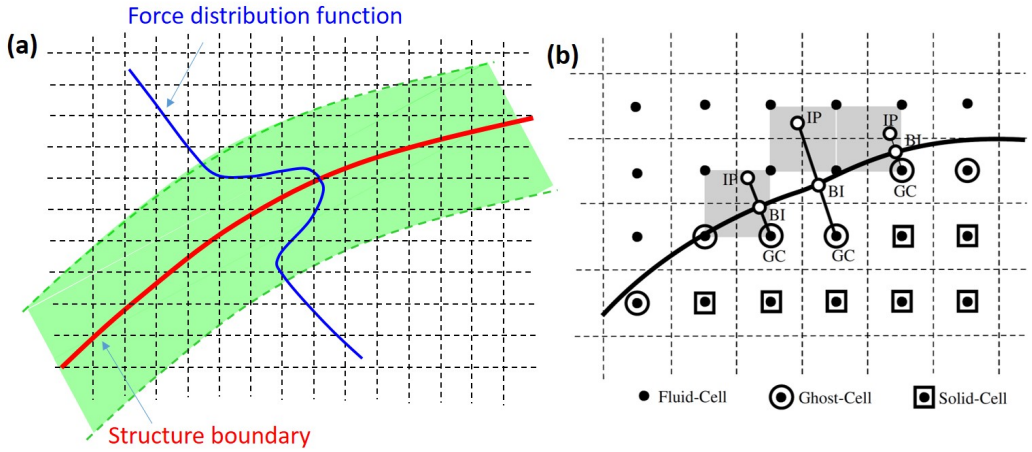

FIG. 3: (a) A force distribution function shown across a structure boundary in continuous forcing IB method and shaded region shows the extent of the force (b) Ghost cell (GC) methodology described by Mittal et al.[44] in discrete forcing IB method (reprinted with permission from Elsevier, copyright 2008[44]).

The temperature T at the IP is expressed in three-dimensional problems by employing a tri-linear interpolation[44] of the form

$$T(x,y,z) = c_1xyz + c_2xy + c_3yz + c_4xz + c_5x + c_6y + c_7z + c_8 \tag{22}$$

where the IP is surrounded by 8 nodes. For a 2D geometry, bilinear interpolation can be used with 4 neighboring cells. There are eight unknown coefficients in the above equation, and these are expressed in terms of the values of T at the 8 neighbouring nodes as follows:

$$T_{\text{IP}} = \sum_{i=1}^{8} \beta_i T_i \tag{23}$$

where β_i are function of coefficients c_i and location of the IP relative to the surrounding nodes. A Dirichlet boundary condition for the temperature at the BI can be prescribed as follows:

$$T_{\text{BI}} = \frac{1}{2}(T_{\text{IP}} + T_{\text{GC}}) \tag{24}$$

In an implicit time-discretization Eq. 24 is written as,

$$T_{\text{GC}} + \sum_{i=1}^{8} \beta_i T_i = 2T_{\text{BI}} \tag{25}$$

and is solved in a coupled manner with the temperature at the surrounding nodes.

For Neumann boundary condition, the following central-difference scheme is used to

express the heat flux on the boundary:

$$-\frac{\dot{q}_w}{k} = \left(\frac{\partial T}{\partial n}\right)_{\text{BI}} = \frac{T_{\text{IP}} - T_{\text{GC}}}{\Delta l} \tag{26}$$

where the heat flux $\dot{q}_w$ [Wm^{-2}] is known at the IB, Δl is the distance between GC and IP and $\vec{n}$ is normal direction unit vector to the IB. Thus, the Neumann boundary condition using Eqs. 23 and 26 is expressed as follows,

$$T_{\text{GC}} - \sum_{i=1}^{8} \beta_i T_i = \triangle l \frac{\dot{q}_w}{k} \tag{27}$$

The Robin boundary condition, Eq. 6, can be discretized along similar lines and expressed as follows,

$$\left(\frac{k}{\triangle l} - \frac{h}{2}\right) T_{\text{GC}} = \left(\frac{k}{\triangle l} + \frac{h}{2}\right) \sum_{i=1}^{8} \beta_i T_i - hT_\infty \tag{28}$$

A similar formulation can be carried out for Robin boundary condition for heat loss due to radiation.

The implementation of Dirichlet and Neumann heat transfer boundary conditions using the ghost cell method was carried out by Pan[86,87] and Luo et al.[88,89] for simple and complex structures boundaries. Inspired by higher-order reconstruction of ghost cell method of Seo and Mittal[90], a third-order ghost cell based method was implemented by Xia et al.[82,91] for enforcing the boundary conditions. Similar interpolation schemes were used in other several studies (e.g. Ref.[92]) in this theme. Xia et al.[82] compared results for the third-order order ghost cell method with the continuous forcing method. They concluded that the former requires only one-third of grid points as compared to the latter, to obtain the same accuracy for forced convection problems.

The implementation of conjugate heat transfer boundary conditions (Eqs. 8 and 9) at the IB have been attempted by previous studies using mirror GC and mirror IP points in the solid domain (Fig. 4). Eq. 27 can be rewritten for the GC in the solid domain as follows,

$$T^*_{\text{GC}} = \sum_{i=1}^{8} \beta^*_i T^*_i + \Delta l \frac{\dot{q}_w}{k^*} \tag{29}$$

where subscripts $*$ corresponds to the properties/variables for the solid. Using Eqs. 9, 27 and 29, we obtain the following equation,

$$kT_{\text{GC}} - k \sum_{i=1}^{8} \beta_i T_i = k^* T^*_{\text{GC}} - k^* \sum_{i=1}^{8} \beta^*_i T^*_i \tag{30}$$

Using Eqs. 8 and 25, we write an expression, connecting temperature at GC in fluid and

solid domain, as follows,

$$T_{\mathrm{GC}} + \sum_{i=1}^{8} \beta_i T_i = T^*_{\mathrm{GC}} + \sum_{i=1}^{8} \beta^*_i T^*_i \tag{31}$$

Eliminating T^*_{GC} from Eqs. 30 and 31, we write the final expression of temperature at GC in fluid domain as follows,

$$(k - k^*) T_{\mathrm{GC}} = (k + k^*) \sum_{i=1}^{8} \beta_i T_i - 2k^* \sum_{i=1}^{8} \beta^*_i T^*_i \tag{32}$$

The above framework for the conjugate heat transfer boundary condition can be readily implemented in a ghost cell method.

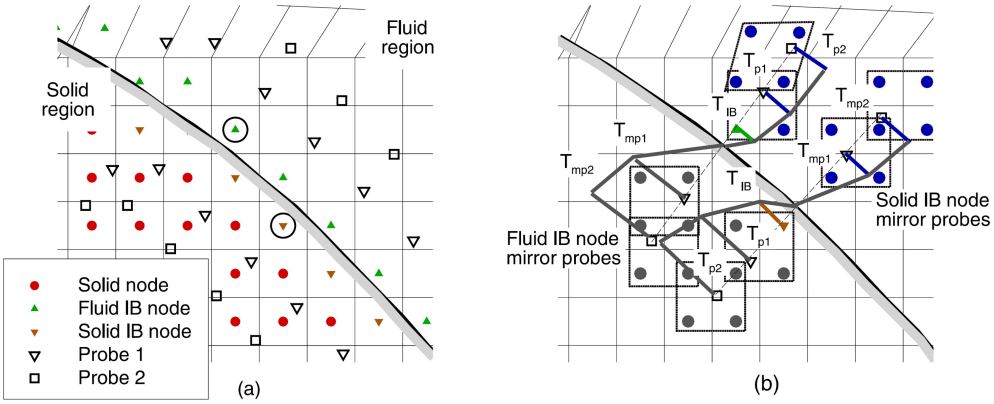

FIG. 4: Conjugate heat transfer boundary condition treatment at the structure boundary by using mirror ghost nodes in the fluid domain and mirror probe points in solid domain, as proposed by Nagendra et al.[93]. Ghost nodes are named as IB node in the figure. (a) Location of nodes in solid and fluid region. (b) Interpolation nodes used in the solid and fluid regions (reprinted with permission from Elsevier, copyright 2014[93]).

The first implementation of conjugate heat transfer in a discrete-forcing IB method was reported by Iaccarino and co-workers[94,95]. In their work, Eqs. 8 and 9 were asymmetrically enforced at the solid and fluid domains. Eq. 8 was prescribed at the fluid domain boundary while Eq. 9 was applied at the solid domain boundary. Authors noted a greater stability of the Dirichlet boundary condition compared to the Neumann boundary condition and a typically larger thermal conductivity of solid than that of fluid, as reasons to prescribe Dirichlet boundary condition at the fluid domain boundary. A higher order interpolation scheme was implemented by Tafti and co-workers[93,96]. In this scheme, two IP points in the fluid domain and two IP points in the structure domain, along with mirror GC in the fluid domain were considered (Fig. 4). Das et al.[19] and Marinis et al.[97] implemented a similar

interpolations that employed two IP points and one IP point, respectively. The convergence of these conjugate heat transfer solvers depends upon the problem parameters[98].

2.3 Applications

In the last two decades, IB methods have been applied to a variety of heat transfer problems, namely, forced convection, natural/mixed convection, mixed convection, conjugate heat transfer an radiation/combustion. The following sub-sections describes some of these applications.

2.3.1 Forced convection

Several researchers have developed and employed continuous forcing based IB methods for heat transfer[69–75,79,81,82]. Paul et al.[72] reported a finite-difference based continuous-forcing IB solver for laminar forced convective heat transfer from an elliptic cylinder. They considered several cylinder axis-ratios, Reynolds numbers and angles-of-attack. Chand et al.[99] employed a diffuse IB method to simulate and quantify the effect of wall roughness on turbulent Rayleigh–Bénard convection.

Regarding discrete forcing IB methods, Kim and Choi[100] proposed an indirect boundary condition imposition IB flow and heat transfer solver, based on a finite-volume discretization on a staggered-grid mesh. They utilized second-order linear and bilinear interpolations[85] to implement Dirichlet and Neumann boundary conditions. The solver capability was demonstrated using canonical thermofluids problems such as forced convection from a circular cylinder and mixed convection around two circular cylinders, mounted side-by-side. Pacheco et al.[101] reported an IB method based heat transfer solver based on non-staggered grids. Their indirect boundary condition imposition discrete forcing IB method was based on the algorithm proposed by Mohd-Yusof[46]. In a subsequent study Pacheco et al.[92] employed this solver for fluid flow and heat transfer processes with either Dirichlet, Neumann or Robin boundary conditions in 2D as well as 3D geometries, and demonstrated the second-order accuracy of the solver. Pan developed a ghost cell IB method and compared convective fluid flow over a stationary cylinder at low Reynolds number (O(10-100)) with existing data[86,87]. Xia et al.[82] used a third-order ghost cell method to compute forced convection around a cluster of stationary particles (Fig. 5), and quantified drag coefficient and Nusselt number on the particles as a function of Reynolds numbers.

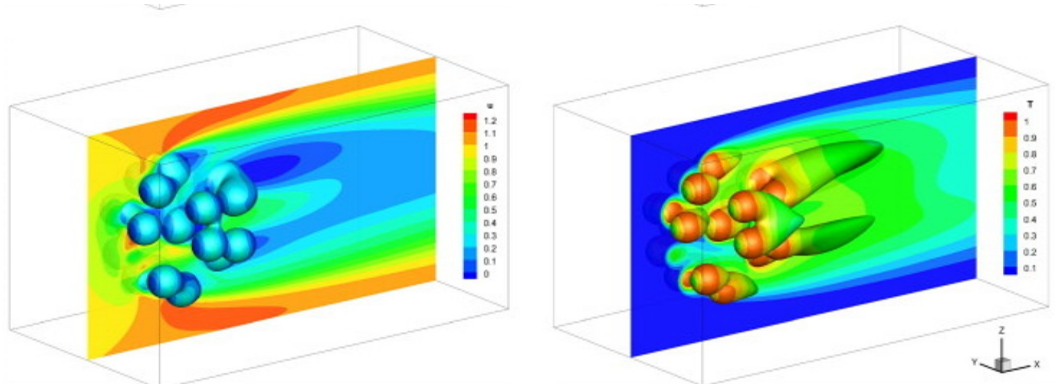

FIG. 5: Computation of flow and temperature field around a cluster of stationary particles[82]. (a) Contours of streamwise velocity in central plane along with iso-surface of T = 0.8. (b) Isotherms in central plane along with iso-surface of u = 0.1 at Re = 100 (reprinted with permission from Elsevier, copyright 2014[82]).

2.3.2 Natural and mixed convection

Shinn et al.[102] used a ghost-cell based IB method to compute shear- and buoyancy-driven flows in cavities of different shapes. Mark et al.[103] demonstrated a discrete forcing IB method for problems involving natural convection. Ashrafizadeh and Hosseinjani[104] employed a discrete forcing IB method[105] to compute convection from two rotating hot cylinders in a cold cavity using a Boussinesq approximation. Recently, based on the ghost cell method of Mittal et al.[44], Garg et al.[106] proposed and validated an IB method with natural and mixed convection in cavity and past a square cylinder. The natural convection was implemented using the Boussinesq approximation in all of these studies.

2.3.3 Conjugate heat transfer

A variety of discrete forcing IB methods have also been developed for problems involving conjugate heat transfer. Iaccarino and co-workers[94,95] developed an IB based solver for high Re flows, which accounts for conjugate heat transfer and mixed convection. They compared the Boussinesq approximation and variable density formulation in these works and found that the latter is preferable in a transitional flow with mixed convection. Fig. 6(a) shows isotherms for flow over a cylinder at one time instance and it highlights the quasi-periodic nature of thermal plumes in the spanwise direction and time[95]. Similarly, Nagendra et al.[93] developed a coupled 3D, conjugate heat transfer solver based on curvilinear grid. Marinis et al.[97] proposed a discrete-forcing IB method for conjugate heat transfer which solved for unsteady Reynolds-averaged Navier–Stokes equations. They applied this method to compute compressible turbulent flow past a turbine vane. Deen and co-workers[19,107] proposed a discrete forcing IB method for convective and conjugate heat transfer through complex porous structures, represented as surfaces with triangular elements on a Cartesian grid (Fig. 6(b, c)).

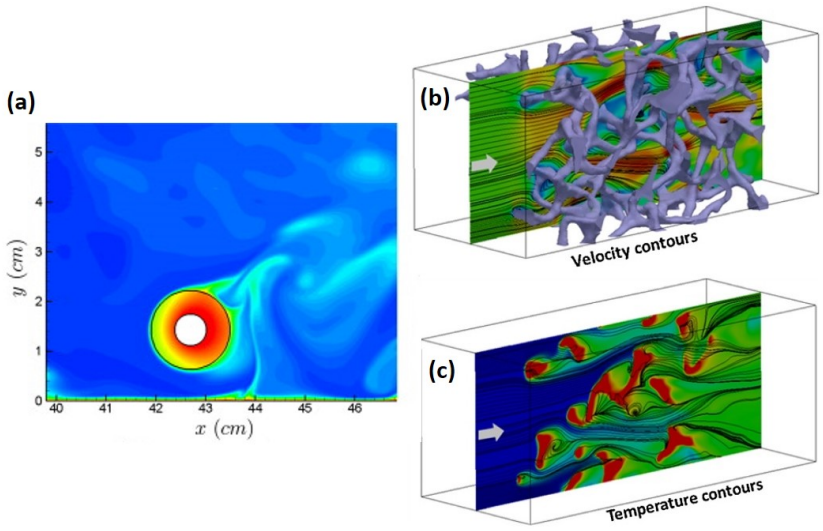

FIG. 6: Instantaneous isotherms are shown in fluid and solid domain in range 284 to 320 K for conjugate heat transfer from a cylinder near a wall[95]. (b, c) Velocity and temperature contours around a complex random solid foam obtained from a conjugate heat transfer simulation on a Cartesian grid[19] (reprinted with permission from Elsevier, copyright 2009[95] and 2016[19]).

2.3.4 Radiation and combustion

Favre et al.[84] proposed a continuous forcing IB method that was extended to simulate problems with conjugate heat transfer taking into account the radiative exchange between surfaces. Lapka and Furmanski[108] proposed a discrete forcing IB method for conjugated radiative-conductive or radiative-convective heat transfer. They were able to model the thermal radiation from highly curved, opaque, or transparent boundaries. Some studies have also tackled combustion using the IB methods. For instance, Kedia et al.[109] proposed a second-order numerical method for computations of reacting flows around thermally conductive solid bodies.The reacting species were modeled using species transport equation and conjugate heat transfer was accounted for with the reacting flow (Fig. 7). Nguyen et al.[4] presented large-eddy simulations (LES) of an internal combustion engine using an IB method. The motion of the valves and the piston was modeled by Lagrangian particles immersed in a stationary Cartesian grid. Measured and computed phase-averaged velocity components were found to be in good agreement in this study.

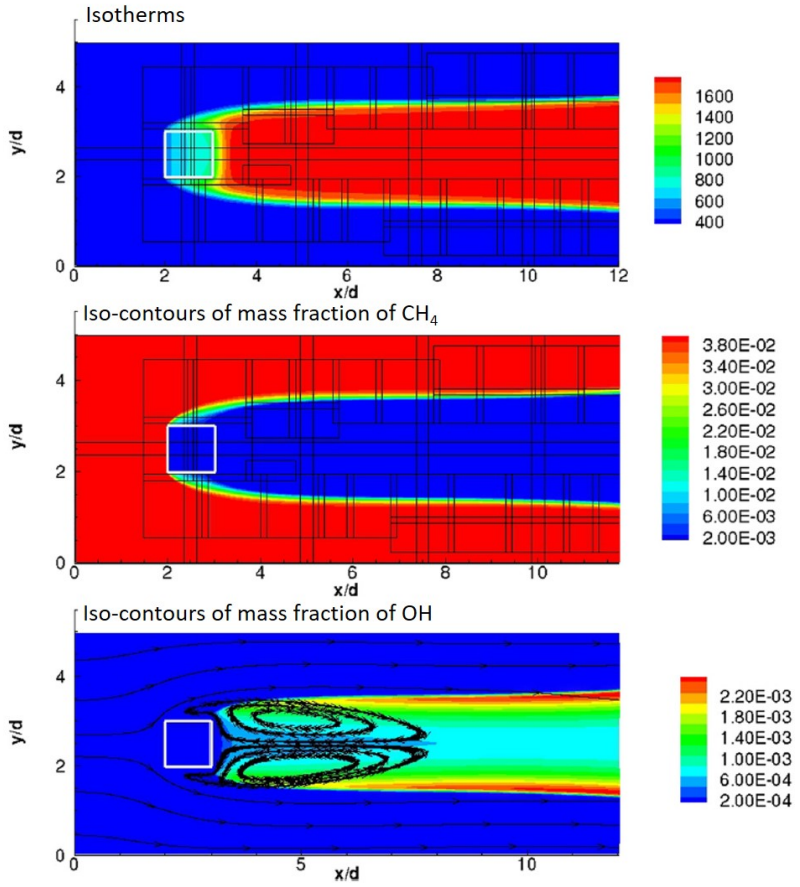

FIG. 7: Computation of stabilization of pre-mixed flame at equivalence ratio of 0.7 on a rectangular cylinder in a channel with blockage ratio and Reynolds number of 0.2 and 1000, respectively [109]. Isotherms, and iso-contours of mass-fraction of methane and intermediate species OH are plotted along with streamlines in different panels. Overlaid fine grid patches are shown in top two panels. (reprinted with permission from Elsevier, copyright 2014 [109]).

3. FLUID-STRUCTURE-THERMAL INTERACTION

3.1 Utilizing FSI to augment convective heat transfer

Interaction of flexible or elastic structures with the flow can be exploited to enhance heat transfer. Often, fluid-structure interaction results in dynamic motion of the structure and this can lead to the shedding of vortices. The interaction of these vortices with the heated wall results in the thinning of the thermal boundary layer and helps to augment the convective heat transfer [7,110,111]. Recent reviews [6,8] have summarized fluid-structure interaction (FSI) studies that have employed flexible plates or piezoelectric fans for convective heat transfer enhancement (Fig. 8). Examples of this abound in biology; for example elephants

flap their large ears to thermoregulate their body temperature[112,113]. These FSI techniques can be categorized into passive and active strategies, which either harness flow energy or utilize an external energy source to augment the heat transfer, respectively. In the former, oscillating bluff bodies inside the channel have been used, while the latter utilized the flow-induced vibration or deformation to enhance heat transfer. For example, Kimber and Garimella[9] experimentally showed that the actuation of thin elastic beam bonded with piezoelectric material enhances convective heat transfer of a hot surface.

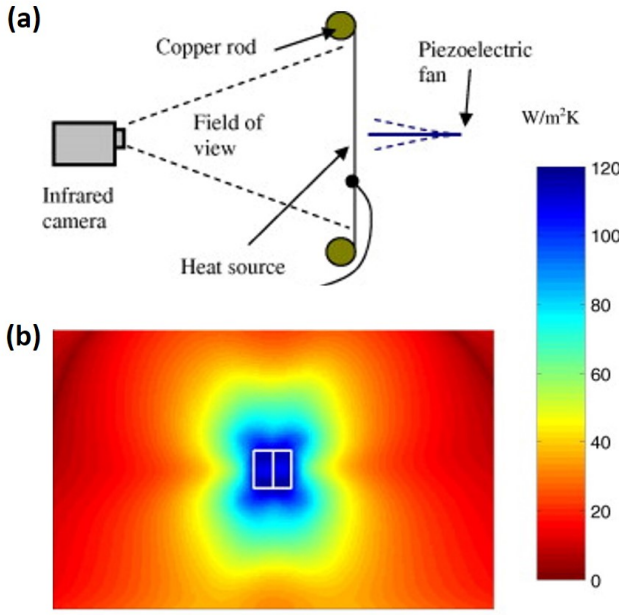

FIG. 8: Piezoelectric fan as an example of a active convective heat transfer augmentation technique[9]. (a) An experimental setup involving infrared thermography employed the fan (b) Iso-contours of heat transfer coefficient on a heated sheet, cooled by a piezoelectric fan (reprinted with permission from Elsevier, copyright 2009[9]).

3.2 Computational challenges

The large deformation of the structure boundary in the fluid flow poses a modeling and computational challenge. The displacement, velocity, and acceleration of a deforming structure may vary strongly with space and time. For instance, a thin splitter plate attached to a cylinder exhibits a non-monotonic displacement along the plate of the length of the plate[114]. In addition, a deforming structure could exhibit material non-linearity or involve complex material model (e.g., a non-linear viscoelastic tissue[115,116]). If the structure is thin (e.g., a membrane or a plate), numerically resolving the stresses in the structure poses a challenge.

Another associated computational challenge with moving boundary computations, especially with sharp-interface IB methods, is spurious pressure oscillations due to ”fresh”

and "dead" cells. The fresh (dead) cells are those fluid (solid) cells which were solid (fluid) cells in the previous time-step. Seo and Mittal[60] developed a "virtual" cut-cell method to enforce regional mass conservation in their ghost-cell sharp interface method[44] which resulted in significant reduction in the pressure oscillations. Griffith and Leontini[117] assessed spurious force oscillations during the movement of the immersed boundary using a sharp-interface IB method. They proposed a heuristic model and recommended that the peak-to-peak distance of any oscillation should be resolved by at least 40 points in case of significant oscillation velocity of the cylinder.

3.3 Governing equations and boundary conditions

The governing equation and boundary conditions for the fluid flow and heat transfer are described in section 2.1. Here we discuss the governing equations for motion of the structure. If a rigid structure is elastically mounted on a spring, its motion is governed by a spring–mass–damper system[118]. If the structure is compliant, the governing equations for the structure, are the Navier equations, with appropriate constitutive material model[119] . In several previous studies, the structure is considered as a Saint Venant-Kirchhoff material which considers geometric non-linearity for a linear elastic material. Regarding boundary conditions, the continuity of velocity and traction are enforced at the structure boundary. The mathematical expressions of the governing equations and boundary conditions can be found in previous papers[24,120].

3.4 Computational approaches

The methods to tackle such class of moving/deforming boundary problems can be broadly classified in two categories, namely, Arbitrary-Lagrangian-Eulerian method (ALE) and IB method. In both methods, the Lagrangian formulation of the Navier equation for structural dynamics is coupled with an Eulerian formulation of the Navier-Stokes equations for the fluid flow. In ALE method, the simulations are carried out on body conformal meshes, which need to be mapped by suitable remeshing algorithm at each time step. This introduced significant complexity[121,122] and as well as additional sources of error and can sometime lead to ill-conditioned discrete systems. On the other hand, a typical IB method, employs a non-body conformal fixed Cartesian (or curvilinear) grid. The governing equations of fluid flow and heat transfer are solved on the fixed uniform/non-uniform Cartesian grid (i.e. within a Eulerian framework), whereas the moving immersed structure boundary, may be solved with a typical body-conformal, finite-element method[114].

The coupling of the flow and structural solvers can be implemented via a, monolithic or a partitioned (or segregated) approach[119,123]. In monolithic solvers, the governing equations for the flow and structure domains are discretized in a unified formulation and solved simultaneously[119,124]. The formulation and numerical solution of such systems becomes more involved for complex constitutive model for the structure. On the other hand, the partitioned approach allows for the use of existing flow and structural dynamics solvers. However, a challenge is to implement the data exchange between the two solvers in a

computationally efficient manner. Furthermore, the stability requirements for the flow and structural domains might impose very different restrictions on the time-step size, and this might have implications for the computational cost of the solution procedure.

In the partitioned (or segregated) approach, two coupling methods are commonly used: explicit/loose and implicit/strong coupling. Fig. 9 illustrates one viable algorithm to couple the solvers using the implicit approach which involves an iterative procedure until the convergence is achieved between flow and structural solver in a given time-step[7]. The convergence of the coupled system is achieved when the residual of a coupled variable (say velocity of structure boundary) drops below a user-defined value. Different types of coupling schemes were recently reviewed by Sotiropoulos and Yang[24]. While the explicit loose coupling is computationally cheaper, it is subjected to constraint of numerical stability. Implicit coupling usually has more relaxed numerical stability constraints but it may be computationally more expensive per time-step. In general, this constraint depends on structure-fluid density ratio and the implicit coupling is required at low values of density ratios[27,125,126]. Oftentimes, the under-relaxation scheme used in implicit partitioned approach for convergence is computationally expensive. In order to address this issues, several studies[127–130] have successfully implemented and tested dynamic relaxation and demonstrated significant speedup.

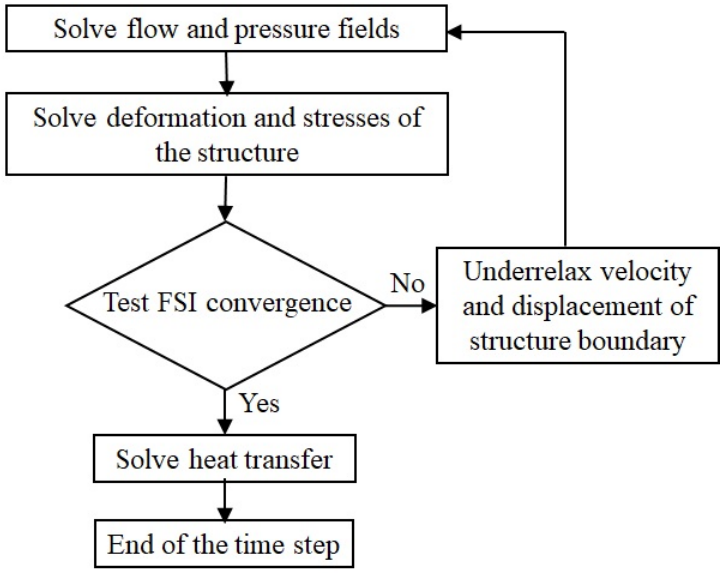

FIG. 9: Algorithm of a partitioned approach for FSI with heat transfer. Solutions of fluid and structure domain are strong coupled and heat transfer is solved after achieving the FSI convergence.

Regarding development of IB methods in this theme, Bhardwaj and Mittal[114] coupled an existing sharp-interface IB method-based flow solver[44] to an open-source finite-element structural solver, Tahoe[131]. This partitioned coupled IB solver was benchmarked against the simulation results of Turek and Hron[120] for flow past a cylinder in a channel with a

flexible splitter plate. Tian et al.[132] validated an IB-based three-dimensional FSI solver for incompressible flows involving large-scale FID. Other immersed interface method-based solvers that simulate large-scale FID have been reported in the last two decades[41,133,134].

3.5 Application to heat transfer with moving boundaries

These problems might involve bodies moving with a prescribed motion or rigid bodies moving under the influence of fluid dynamic forces, or flow-induced deformation of a compliant structure. The first category, i.e. bodies with prescribed motion, are a relatively simple extension of the IB method (see Kumar and Roy[135] for an example) so we focus here on the latter two categories of moving boundary problems..

3.5.1 Rigid bodies moving under the influence of fluid dynamic forces

Feng and Michaelides[136] developed a continuous forcing based IB solver (Proteus) in which forces on non-heated or heated particles, namely, gravity, buoyancy and particle collision forces, could be accounted for. Using Proteus, Feng and Musong[137] presented 3D simulations of forced and mixed convection of rigid spherical particles in particulate flows with a prescribed fluidization velocity (Fig. 10). The particles movement by driven by the equations of linear and angular motion. In a follow-up work, Musong et al.[138] demonstrated a 3D continuous forcing IB method for natural convection encountered during thermal interaction of several particles with fluid flow.

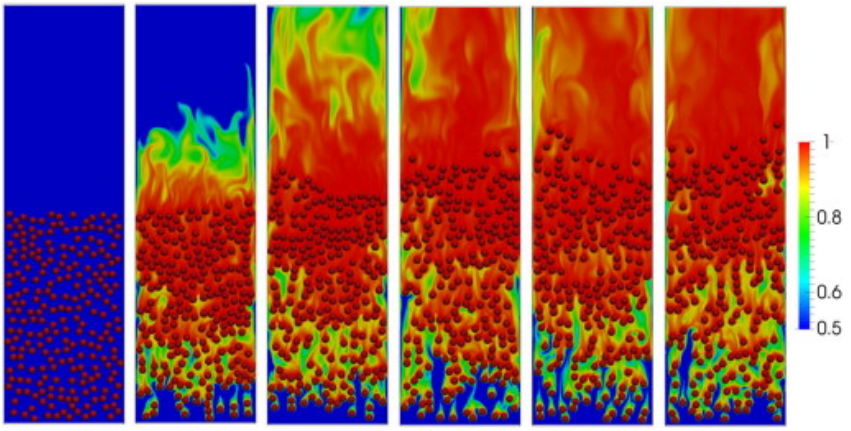

FIG. 10: Computed isotherms in mid vertical plane at different times, with fluidization velocity of 0.05 m/s by Feng and Musong[137] (reprinted with permission from Elsevier, copyright 2014[137]).

Vortex shedding past an elastically-mounted rigid structure such as a bluff-body initiates flow-induced vibrations (FIV) and these vibrations are sustained by the oscillating shear layers and vortices[139]. FIV of bluff structures involving heat transfer is of considerable interest in heat exchangers, chimneys carrying hot gases, hot and cold fluids mixing

in heat transfer devices, and others. The FIV of an elastically mounted circular cylinder has been investigated in detail in previous studies and the FIV can be broadly into vortex-induced vibration (VIV), galloping and flutter[140–142].

Several computational models based on IB methods have investigated VIV of the cylinder in the presence of the heat transfer. Garg et al.[106] developed a sharp-interface immersed boundary method for VIV and galloping of a cylinder in the presence of thermal buoyancy, which employed the Boussinesq model. They showed that VIV of an elastically mounted cylinder can be achieved at a very low Reynolds number by utilizing thermal buoyancy, induced by hot and cold parallel plates oriented along the direction of the flow. Subsequent studies[143–145] showed that the suppression or amplification of VIV can be achieved by thermal buoyancy in different configurations (Fig. 11). Kumar et al.[111] utilized a sharp-interface IB method to simulate VIV and galloping of a D-section cylinder to improve heat transfer in a heated laminar channel flow. They reported that owing to galloping, the D-section cylinder oscillates over an extended range of reduced velocities and spreads detached vortices over larger areas, which helps heat transfer.

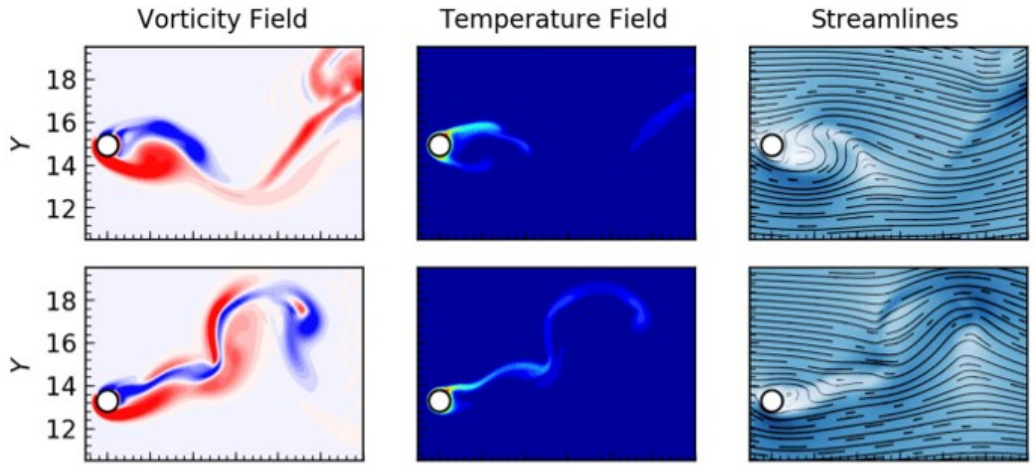

FIG. 11: Mixed convective heat transfer during VIV of a cylinder[144]. Vorticity, temperature fields, and streamlines plotted over a displacement cycle of the cylinder, at the maximum (top row) and minimum (bottom row) cylinder displacement at Re = 150. The values of reduced velocity and Richardson number were 10 and 4, respectively (reprinted with permission from American Institute of Physics, copyright 2019[144])

3.5.2 Flow-induced deformation (FID) of compliant structures

Numerical simulations involving FID of the soft structures with convective heat transfer have been reported recently. Several studies showed the advantage of FID in improving convective heat transfer using high-fidelity computational simulations involving both diffuse-interface and sharp-interface IB methods. Shoele and Mittal[7] used a diffuse-interface IB method (the feedback control method of Goldstein et al.[34]) to simulate the FID of a flexible reed in a confined channel. Soti et al.[110] employed a sharp-interface

IB method (Ghost cell IB method[44]) and examined heat transfer enhancement via large-scale FID of an elastic splitter plate mounted on the lee side of a cylinder, at Reynolds number, Re = 100, and compared the thermal augmentation of configurations with and without FID. In a series of papers, Sung and coworkers employed fluid-structure-thermal interaction between flexible flag(s) and heated channel in different configurations, namely, inverted flag[146], vertically clamped flexible flag[147] and asymmetrically clamped flexible flags[148]. In these studies, they employed a diffuse-interface IB approach of Goldstein et al.[34]. While much of the work in this arena has employed two-dimensional models, Rips et al.[149] carried out 3D fully coupled fluid–structure–thermal simulations using a diffuse-interface IB based method (Fig. 12). Understanding non-isothermal mixing of miscible fluids is another area in which FID could play an important role in improving the mixing efficiency. While there are no reports on IB methods application to non-isothermal mixing, recent studies have successfully invoked IB methods to show the improvement in mixing using flow-induced flutter of a membrane[150,151].

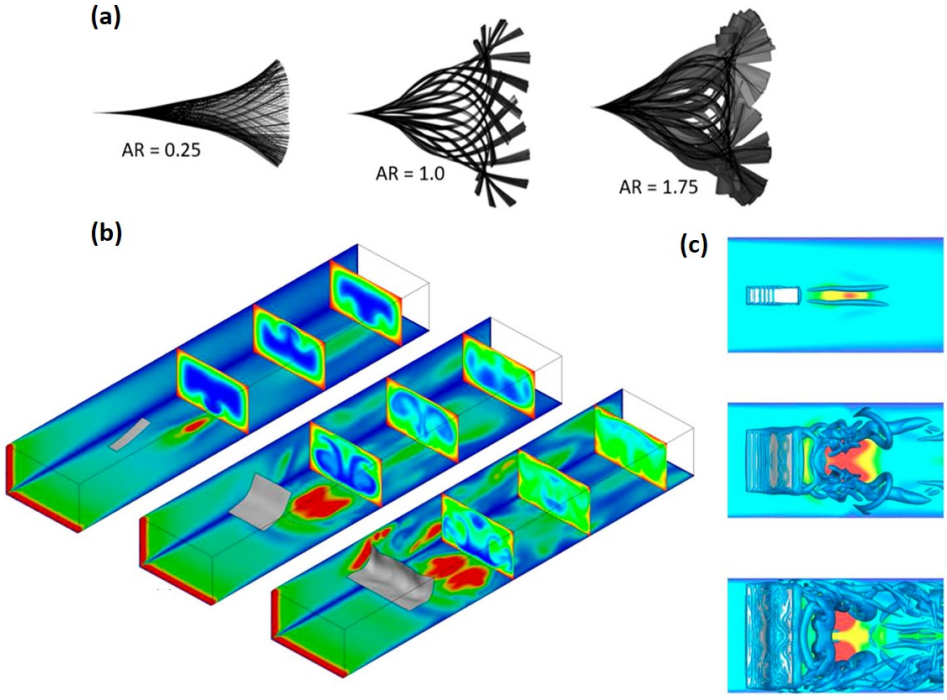

FIG. 12: 3D simulation of a flapping flag in a square duct, deployed for achieving thermal augmentation[149]. (a) Superimposed shapes of flags at different time-instances for different aspect ratio (AR) (b) Computed isotherms on channel walls and on cross-stream planes (c) Vortex structures seen from the top view for the flags of different aspect-ratios (reprinted with permission from American Institute of Physics, copyright 2020[149]).

4. EMERGING TOPICS IN THERMOFLUIDS

4.1 Bioheat transfer

IB methods have been utilized successfully to compute biomedical flows and model problems related to bioheat transfer. In several cancer therapies, heat transfer in the vascular system and its coupling with blood flow are important, and the modeling of these procedures should account for this coupling. Examples of such interventions include cryosurgery[152], hyperthermia[153] and radio frequency ablation[154].

One of the earliest implementation of IB method for bioheat transfer was in the context of cryo-preservation of biological material and was carried out by Mao et al[62]. The authors simulated the response of a cell to freezing and the cell was modeled with a membrane and was surrounded by an aqueous salt solution and ice (Fig. 13(a)). The concentration field of the salt and temperature field in both ice and salt solution were computed in the presence of mass transport through the cell membrane (Fig. 13(b)). Authors used sharp interface IB method, reported earlier in their studies[51,61,63], to simulate the dynamics of the phase boundary.

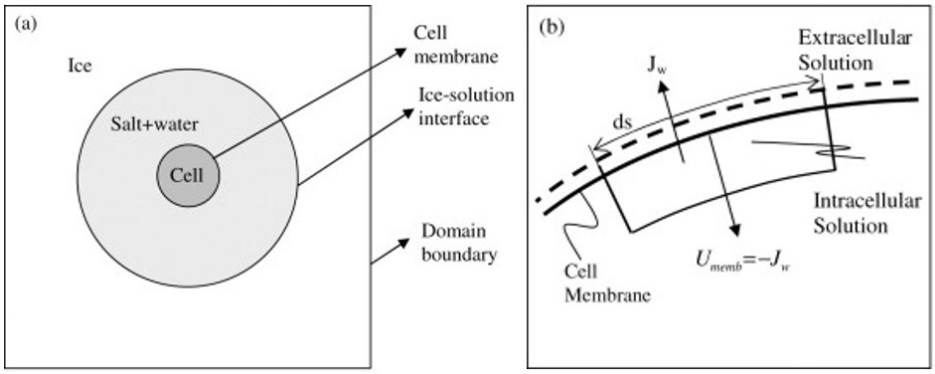

FIG. 13: Schematic of the computational model for the ice–cell interaction problem, considered by Mao et al[62]. (a) The cell and ice–solution interface are placed on a uniform Cartesian mesh and the interfaces are moved over the mesh. A finite volume discretization of the governing equations is performed on the fixed mesh. (b) The computational model for cell membrane (reprinted with permission from Elsevier, copyright 2003[62]).

In the context of simulating tissue cryo-freezing, several studies solved Pennes' bioheat transfer equation[155] in a tissue using IB method. This equation is a modified transient heat conduction equation to account the effect of blood flow and metabolic heat generation rate through the tissue ($\dot{q}_m$ [Wm^{-3}]) and the latter is accounted as a source term in the heat equation, given as follows[68,155]:

$$\rho_t C_t \frac{\partial T}{\partial t} = \frac{\partial}{\partial x_j}\left(k_t \frac{\partial T}{\partial x_j}\right) + \omega \rho_b C_b (T_a - T_t) + \dot{q}_m \tag{33}$$

where subscripts t, b a, and m represent tissue, blood, arterial blood and metabolic, respectively. C is specific heat and ω is perfusion rate (m^3/s of volumetric blood flow per m^3 of tissue).

Ge et al.[156] solved Pennes equation in two-dimensional coordinates using a finite-difference based, continuous forcing IB method, in which temperature-dependent thermophysical properties of the tissue were accounted for and heating effect due to blood flow was imposed using boundary condition at IB. Using this IB based solver[156], the authors investigated the effects of injected nanoparticles and blood vessel structure during cryosurgery. Further, they computed the temperature field during cryosurgery in a complex blood vascular system for different tumor locations[157]. Ge et al.[16] compared data obtained by three-dimensional extension of their IB solver[156] with *in vitro* experiments and found a good agreement between the two (Fig. 14). In the arena of radio frequency ablation, Shao et al.[158] modeled thermal effects in branched networks of vascular system and solved Pennes bioheat equation using a continuous forcing IB method, reported earlier in their works[70,156].

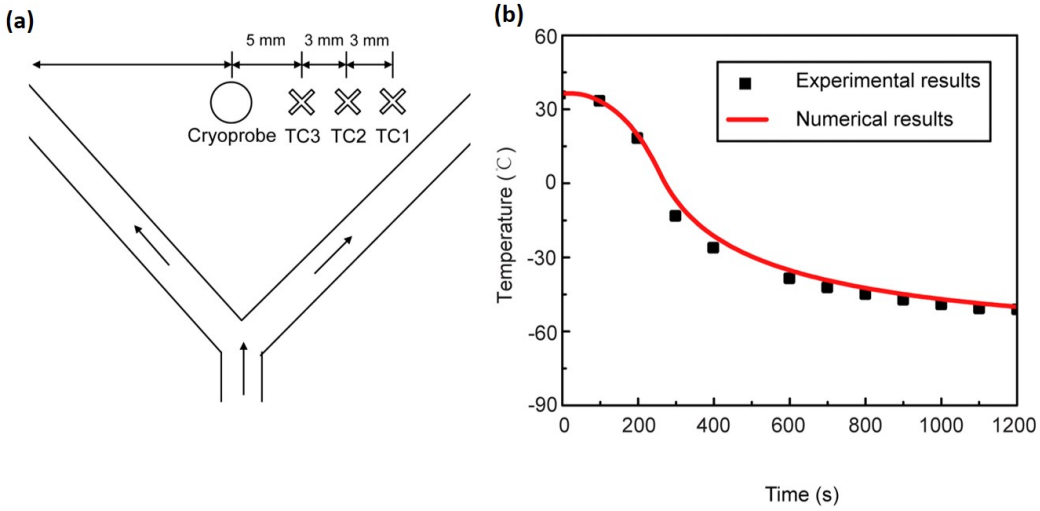

FIG. 14: Comparison of IB computations with *in vitro* experiments[16] (a) Schematic showing location of thermocouples (TC) and cryoprobe, with Y-shape blood vessel. (b) Computed between measured and computed time-varying temperature by IB solver at TC1 (reprinted with permission from Elsevier, copyright 2017[16]).

4.2 High-Speed Compressible Flows

Heat transfer naturally appears as an important component of all high-speed compressible flows and transfer of heat between the fluid and the immersed structure/body is important in many applications[159,160]. The progress in IB methods for compressible flows was briefly summarized in a recent review[28]. The development of IB methods for supersonic and hypersonic flows started with extension of discrete-forcing IB methods to subsonic

compressible flows. In the context of subsonic compressible flows, Palma et al.[161] developed a discrete-forcing method for solving the compressible Reynolds-averaged Navier-Stokes equations and simulated subsonic flow past a heated cylinder as well as supersonic flows past an airfoil and a circular cylinder. Ghias et al.[54] proposed a second-order accurate ghost cell method for viscous compressible flows for Cartesian or curvilinear grids. Using a higher order ghost cell scheme of Seo and Mittal[90], Bailoor et al.[162] proposed a FSI solver for subsonic compressible flows with large-scale FID of a thin structure. Similarly, Wang et al.[163] demonstrated IB method for large-scale FID with compressible multiphase flows. Previous studies[164,165] have employed a sharp-interface IB method for simulating FID of the human eye subject to the loading from a blast-induced shock wave with a subsonic Mach number.

For supersonic flows, Chaudhuri et al.[166] described the methodology of a ghost cell based IB method, in which authors used a quadratic interpolation scheme to find the value of GC. The solver was validated against analytical solution of supersonic flow past triangular prism and circular cylinder and previous experimental results. Shock-obstacle interaction were simulated at a Mach number of 3.5 in this study (Fig. 15). Kumar et al.[167] implemented the ghost-cell method proposed by Mittal et al.[44] in a central upwind scheme and demonstrated second-order accuracy for their IB based solver. They applied the solver to invisid supersonic flow at Mach number of 3.0 and viscous supersonic flows at Mach number of 1.2 and 2.0. for canonical fluid flow problems such as flow around a circular cylinder.

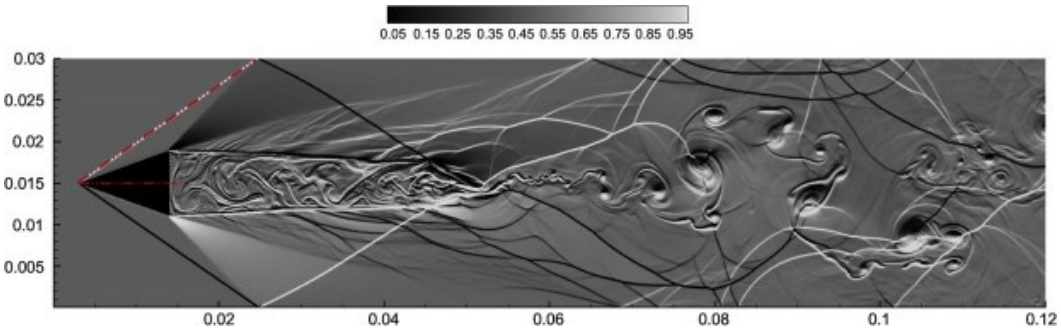

FIG. 15: Numerical schlieren picture for supersonic flow past circular cylinder for a Mach number of 3.5[166] (reprinted with permission from Elsevier, copyright 2011[166].

In the context of the hypersonics flows, one main challenge in this arena is to treat shock discontinuity near or in contact with the IB at high Mach numbers. Greene et al.[168,169] demonstrated a cut-cell IB method for computing flows involving hypersonic boundary layers and used a fifth-order weighted essentially non-oscillatory scheme. Inspired by their earlier work[170], they "dropped" grid points in the computation, which are too close to the IB, relieving the constraint of the limiting time-step due to these grid points. A classification of the grid points used in these works is reproduced in Fig. 16.

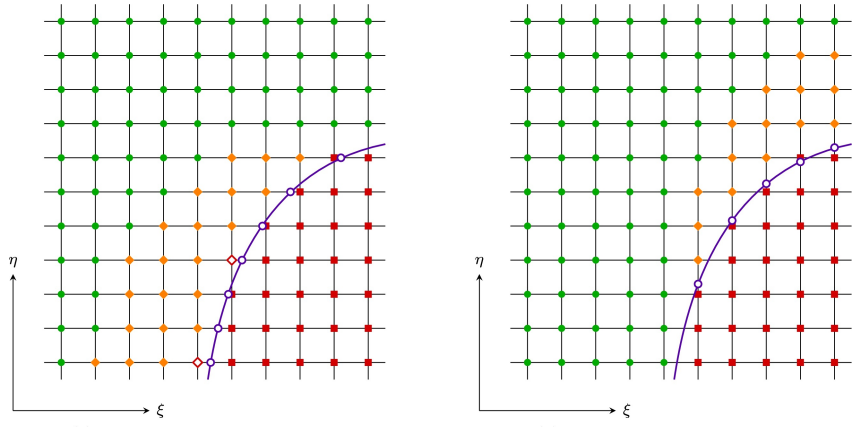

(a) Point classification for ξ direction. (b) Point classification for η direction.

FIG. 16: Classification of grid points for a 2D domain[168] in both corrdinates (b, c). IB(purple line), Regular points (green circles), irregular point (orange diamonds), boundary points (purple hollow circles), dropped point in both directions (red circles) and dropped point in specified direction (red hollow diamonds) are shown (reprinted with permission from Elsevier, copyright 2016[168]).

To alleviate the shock discontinuity close to IB, Bridel-Bertomeu[171] proposed a ENO-like weighted least-square approach scheme in a ghost cell based IB method to handle the interpolation in region with discontinuities. In this scheme, a smoother sub-stencil is extracted from the baseline interpolation stencil to construct a robust interpolation scheme. This scheme is inspired from a revised ENO scheme of[172], which uses a data-dependent weighted least-squares reconstruction with a fixed stencil,in which weights are chosen to render smooth data during the reconstruction. The solver allowed them to capture hypersonic flows with strong discontinuities near or in contact with the IB and was demonstrated by simulating canonical hypersonic flows (Fig. 17). Brahmachary et al.[173] presented a sharp interface IB method on an unstructured Cartesian mesh framework for viscous hypersonic flows. They showed that solution reconstruction plays a more important role than grid resolution while computing heat flux on the wall.

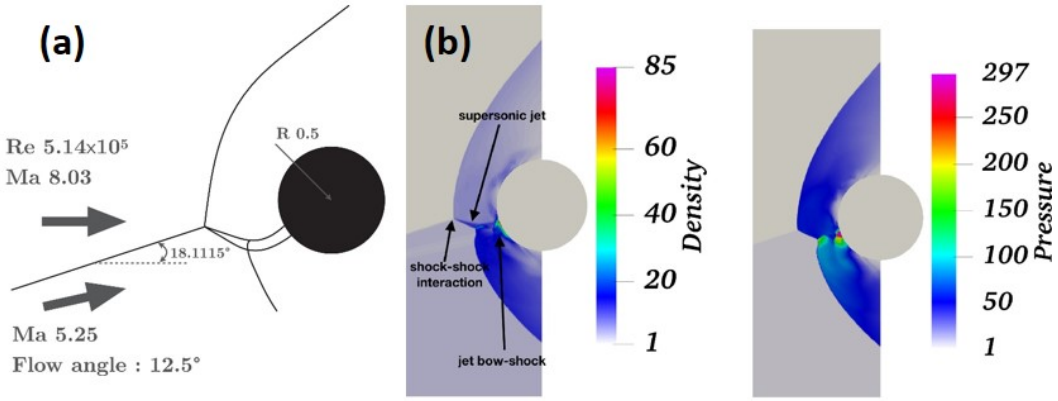

FIG. 17: Computation of shock-shock interaction near to a surface in hypersonics[171] (a) Problem definition with flow configuration (b) Computed density contours exhibiting shock-shock interaction (c) Computed pressure contours (reprinted with permission from Elsevier, copyright 2021[171]).

5. CLOSURE AND FUTURE OUTLOOK

We have reviewed the development and application of immersed boundary (IB) methods to thermofluids problems. We provide a brief overview and classification of IB methods along with a discussion of the advantages that these methods afford over other methods. Early developments in the context of development of IB methods for thermofluids problems are discussed. The governing equations and boundary conditions have been presented. We discuss implementation strategies for the common thermal boundary conditions of prescribed temperature, prescribed heat flux, and convective and radiative loss from a solid boundary in the context of continuous as well as discrete forcing IB methods. We have reviewed several studies in which IB methods for thermofluids were implemented in different heat transfer scenarios. Both stationary and moving boundary problems are discussed. In the latter category, which is particularly suitable for the application of IB methods, we review previous IB based studies in motion induced in rigid solids by fluid-dynamic forces as well as flow-induced deformation of compliant structures. The computational challenges, approaches and studies demonstrating convective heat transfer enhancement using flow-induced deformation, were summarized in this review as well. Lastly, we have briefly reviewed developments related to IB methods in two emerging areas in thermofluids, namely, bioheat transfer, and high-speed compressible flows.

6. ACKNOWLEDGEMENTS

R.M. acknowledges support from US National Science Foundation (grants CBET-1738918, PHY-1806689, DUE-1734744, CBET-2019405 and CBET-1357819) and US Airforce Office of Scientific Research. R.B. acknowledges financial support from Science and Engineering Research Board (SERB, grant # MTR/2019/000696), Department of Science and Technology (DST), New Delhi, India.

REFERENCES

1. Ali, H.M., Saieed, A., Pao, W., Ali, M., , Copper foam/PCMs based heat sinks: an experimental study for electronic cooling systems, International Journal of Heat and Mass Transfer, vol. **127**, pp. 381–393, 2018.
2. Bhutta, M.M.A., Hayat, N., Bashir, M.H., Khan, A.R., Ahmad, K.N., and Khan, S., CFD applications in various heat exchangers design: A review, Applied Thermal Engineering, vol. **32**, pp. 1–12, 2012.
3. Cho, J., Yang, J., and Park, W., Evaluation of air distribution system's airflow performance for cooling energy savings in high-density data centers, Energy and buildings, vol. **68**, pp. 270–279, 2014.

4. Nguyen, T., Proch, F., Wlokas, I., and Kempf, A., Large eddy simulation of an internal combustion engine using an efficient immersed boundary technique, Flow, Turbulence and Combustion, vol. **97**, no. 1, pp. 191–230, 2016.
5. Tang, C., Courtesy of NASA/Ames, https://www.nas.nasa.gov/SC15/demos/demo15.html, Retrieved in September 2021.
6. Gallegos, R.K.B. and Sharma, R.N., Flags as vortex generators for heat transfer enhancement: Gaps and challenges, Renewable and Sustainable Energy Reviews, vol. **76**, pp. 950–962, 2017.
7. Shoele, K. and Mittal, R., Computational study of flow-induced vibration of a reed in a channel and effect on convective heat transfer, Physics of Fluids, vol. **26**, no. 12, p. 127103, 2014.
8. Hales, A. and Jiang, X., A review of piezoelectric fans for low energy cooling of power electronics, Applied Energy, vol. **215**, pp. 321–337, 2018.
9. Kimber, M. and Garimella, S.V., Measurement and prediction of the cooling characteristics of a generalized vibrating piezoelectric fan, International Journal of Heat and Mass Transfer, vol. **52**, no. 19-20, pp. 4470–4478, 2009.
10. Shyy, W., Udaykumar, H., and Rao, M.M., Computational fluid dynamics with moving boundaries, CRC Press, 1995.
11. Kapahi, A., Sambasivan, S., and Udaykumar, H., A three-dimensional sharp interface Cartesian grid method for solving high speed multi-material impact, penetration and fragmentation problems, Journal of Computational Physics, vol. **241**, pp. 308–332, 2013.
12. Yeoh, G.H. and Tu, J., Computational techniques for multiphase flows, Butterworth-Heinemann, 2019.
13. Hu, J., Xu, J., Zhu, C., Li, Q., Ullah, Z., Liu, F., Li, W., Guo, Y., Zhao, X., and Liu, L., Significant enhancement of metal heat dissipation from mechanically exfoliated graphene nanosheets through thermal radiation effect, AIP Advances, vol. **7**, no. 5, p. 055315, 2017.
14. Weissenböck, N.M., Weiss, C.M., Schwammer, H.M., and Kratochvil, H., Thermal windows on the body surface of African elephants (Loxodonta africana) studied by infrared thermography, Journal of Thermal Biology, vol. **35**, no. 4, pp. 182–188, 2010.
15. Mccafferty, D.J., Gilbert, C., Thierry, A.M., Currie, J., Le Maho, Y., and Ancel, A., Emperor penguin body surfaces cool below air temperature, Biology letters, vol. **9**, no. 3, p. 20121192, 2013.
16. Ge, M., Shu, C., Yang, W., and Chua, K., Incorporating an immersed boundary method to study thermal effects of vascular systems during tissue cryo-freezing, Journal of thermal biology, vol. **64**, pp. 92–99, 2017.
17. Ocko, S.A. and Mahadevan, L., Collective thermoregulation in bee clusters, Journal of The Royal Society Interface, vol. **11**, no. 91, p. 20131033, 2014.
18. Albrecht, H., Fiorani, F., Pieruschka, R., Müller-Linow, M., Jedmowski, C., Schreiber, L., Schurr, U., and Rascher, U., Quantitative estimation of leaf heat transfer coefficients by active thermography at varying boundary layer conditions, Frontiers in plant science, vol. **10**, p. 1684, 2020.
19. Das, S., Deen, N.G., and Kuipers, J., Direct numerical simulation for flow and heat transfer through random open-cell solid foams: Development of an IBM based CFD model, Catalysis Today, vol. **273**, pp. 140–150, 2016.

20. Souli, M., Ouahsine, A., and Lewin, L., ALE formulation for fluid–structure interaction problems, Computer methods in applied mechanics and engineering, vol. **190**, no. 5-7, pp. 659–675, 2000.
21. Peskin, C.S., The immersed boundary method, Acta numerica, vol. **11**, pp. 479–517, 2002.
22. Mittal, R. and Iaccarino, G., Immersed boundary methods, Annual Review of Fluid Mechanics, vol. **37**, pp. 239–261, 2005.
23. Iaccarino, G. and Verzicco, R., Immersed boundary technique for turbulent flow simulations, Appl. Mech. Rev., vol. **56**, no. 3, pp. 331–347, 2003.
24. Sotiropoulos, F. and Yang, X., Immersed boundary methods for simulating fluid–structure interaction, Progress in Aerospace Sciences, vol. **65**, pp. 1–21, 2014.
25. Griffith, B.E. and Patankar, N.A., Immersed methods for fluid–structure interaction, Annual review of fluid mechanics, vol. **52**, pp. 421–448, 2020.
26. Hou, G., Wang, J., and Layton, A., Numerical methods for fluid-structure interaction–a review, Communications in Computational Physics, vol. **12**, no. 2, pp. 337–377, 2012.
27. Kim, W. and Choi, H., Immersed boundary methods for fluid-structure interaction: A review, International Journal of Heat and Fluid Flow, vol. **75**, pp. 301–309, 2019.
28. Huang, W.X. and Tian, F.B., Recent trends and progress in the immersed boundary method, Proceedings of the Institution of Mechanical Engineers, Part C: Journal of Mechanical Engineering Science, vol. **233**, no. 23-24, pp. 7617–7636, 2019.
29. Xiao, W., Zhang, H., Luo, K., Mao, C., and Fan, J., Immersed boundary method for multiphase transport phenomena, Reviews in Chemical Engineering, 2020.
30. Peskin, C.S., Flow patterns around heart valves: a numerical method, Journal of computational physics, vol. **10**, no. 2, pp. 252–271, 1972.
31. Peskin, C.S., Flow patterns around heart valves: a digital computer method for solving the equations of motion, Yeshiva University, 1972.
32. Peskin, C.S., Numerical analysis of blood flow in the heart, Journal of computational physics, vol. **25**, no. 3, pp. 220–252, 1977.
33. Peskin, C.S., The fluid dynamics of heart valves: experimental, theoretical, and computational methods, Annual review of fluid mechanics, vol. **14**, no. 1, pp. 235–259, 1982.
34. Goldstein, D., Handler, R., and Sirovich, L., Modeling a no-slip flow boundary with an external force field, Journal of computational physics, vol. **105**, no. 2, pp. 354–366, 1993.
35. Unverdi, S.O. and Tryggvason, G., A front-tracking method for viscous, incompressible, multi-fluid flows, Journal of computational physics, vol. **100**, no. 1, pp. 25–37, 1992.
36. Juric, D. and Tryggvason, G., A front-tracking method for dendritic solidification, Journal of computational physics, vol. **123**, no. 1, pp. 127–148, 1996.
37. Glowinski, R., Pan, T.W., and Periaux, J., A fictitious domain method for Dirichlet problem and applications, Computer Methods in Applied Mechanics and Engineering, vol. **111**, no. 3-4, pp. 283–303, 1994.
38. Uhlmann, M., An immersed boundary method with direct forcing for the simulation of particulate flows, Journal of Computational Physics, vol. **209**, no. 2, pp. 448–476, 2005.
39. Angot, P., Bruneau, C.H., and Fabrie, P., A penalization method to take into account obstacles in incompressible viscous flows, Numerische Mathematik, vol. **81**, no. 4, pp. 497–520, 1999.

40. Wang, X. and Liu, W.K., Extended immersed boundary method using FEM and RKPM, Computer Methods in Applied Mechanics and Engineering, vol. **193**, no. 12-14, pp. 1305–1321, 2004.
41. Zhang, L., Gerstenberger, A., Wang, X., and Liu, W.K., Immersed finite element method, Computer Methods in Applied Mechanics and Engineering, vol. **193**, no. 21-22, pp. 2051–2067, 2004.
42. Ye, T., Mittal, R., Udaykumar, H., and Shyy, W., An accurate Cartesian grid method for viscous incompressible flows with complex immersed boundaries, Journal of computational physics, vol. **156**, no. 2, pp. 209–240, 1999.
43. Udaykumar, H., Mittal, R., Rampunggoon, P., and Khanna, A., A sharp interface Cartesian grid method for simulating flows with complex moving boundaries, Journal of computational physics, vol. **174**, no. 1, pp. 345–380, 2001.
44. Mittal, R., Dong, H., Bozkurttas, M., Najjar, F., Vargas, A., and von Loebbecke, A., A versatile sharp interface immersed boundary method for incompressible flows with complex boundaries, Journal of Computational Physics, vol. **227**, pp. 4825–4852, 2008.
45. LeVeque, R.J. and Li, Z., The immersed interface method for elliptic equations with discontinuous coefficients and singular sources, SIAM Journal on Numerical Analysis, vol. **31**, no. 4, pp. 1019–1044, 1994.
46. Mohd-Yusof, J., Combined immersed-boundary/B-spline methods for simulations of flow in complex geometries, Center for turbulence research annual research briefs, vol. **161**, no. 1, pp. 317–327, 1997.
47. Fadlun, E., Verzicco, R., Orlandi, P., and Mohd-Yusof, J., Combined immersed-boundary finite-difference methods for three-dimensional complex flow simulations, Journal of computational physics, vol. **161**, no. 1, pp. 35–60, 2000.
48. Melton, J., Berger, M., Aftosmis, M., and Wong, M., 3d applications of a cartesian grid euler method, In 33rd aerospace sciences meeting and exhibit, p. 853, 1995.
49. Udaykumar, H.S., Shyy, W., and Rao, M.M., Elafint: a mixed Eulerian–Lagrangian method for fluid flows with complex and moving boundaries, International journal for numerical methods in fluids, vol. **22**, no. 8, pp. 691–712, 1996.
50. Udaykumar, H.S., Kan, H.C., Shyy, W., and Tran-Son-Tay, R., Multiphase dynamics in arbitrary geometries on fixed Cartesian grids, Journal of Computational Physics, vol. **137**, no. 2, pp. 366–405, 1997.
51. Udaykumar, H., Mao, L., and Mittal, R., A finite-volume sharp interface scheme for dendritic growth simulations: comparison with microscopic solvability theory, Numerical Heat Transfer: Part B: Fundamentals, vol. **42**, no. 5, pp. 389–409, 2002.
52. Majumdar, S., Iaccarino, G., Durbin, P., , RANS solvers with adaptive structured boundary non-conforming grids, Annual Research Briefs, vol. **1**, 2001.
53. Tseng, Y.H. and Ferziger, J.H., A ghost-cell immersed boundary method for flow in complex geometry, Journal of computational physics, vol. **192**, no. 2, pp. 593–623, 2003.
54. Ghias, R., Mittal, R., and Dong, H., A sharp interface immersed boundary method for compressible viscous flows, Journal of Computational Physics, vol. **225**, no. 1, pp. 528–553, 2007.
55. Roma, A.M., Peskin, C.S., and Berger, M.J., An adaptive version of the immersed boundary method, Journal of computational physics, vol. **153**, no. 2, pp. 509–534, 1999.

56. Peng, Y.F., Mittal, R., Sau, A., and Hwang, R.R., Nested Cartesian grid method in incompressible viscous fluid flow, Journal of Computational Physics, vol. **229**, no. 19, pp. 7072–7101, 2010.
57. Vanella, M., Rabenold, P., and Balaras, E., A direct-forcing embedded-boundary method with adaptive mesh refinement for fluid–structure interaction problems, Journal of Computational Physics, vol. **229**, no. 18, pp. 6427–6449, 2010.
58. Udaykumar, H., Krishnan, S., and Marella, S.V., Adaptively refined, parallelised sharp interface Cartesian grid method for three-dimensional moving boundary problems, International Journal of Computational Fluid Dynamics, vol. **23**, no. 1, pp. 1–24, 2009.
59. Meyer, M., Devesa, A., Hickel, S., Hu, X., and Adams, N.A., A conservative immersed interface method for large-eddy simulation of incompressible flows, Journal of Computational Physics, vol. **229**, no. 18, pp. 6300–6317, 2010.
60. Seo, J.H. and Mittal, R., A sharp-interface immersed boundary method with improved mass conservation and reduced spurious pressure oscillations, Journal of computational physics, vol. **230**, no. 19, pp. 7347–7363, 2011.
61. Udaykumar, H. and Mao, L., Sharp-interface simulation of dendritic solidification of solutions, International journal of heat and mass transfer, vol. **45**, no. 24, pp. 4793–4808, 2002.
62. Mao, L., Udaykumar, H., and Karlsson, J., Simulation of micro-scale interaction between ice and biological cells, International journal of heat and mass transfer, vol. **46**, no. 26, pp. 5123–5136, 2003.
63. Udaykumar, H., Mittal, R., and Shyy, W., Computation of solid–liquid phase fronts in the sharp interface limit on fixed grids, Journal of computational physics, vol. **153**, no. 2, pp. 535–574, 1999.
64. Shyy and, W., Francois, M., Udaykumar, H., N'dri and, N., and Tran-Son-Tay, R., Moving boundaries in micro-scale biofluid dynamics, Appl. Mech. Rev., vol. **54**, no. 5, pp. 405–454, 2001.
65. Francois, M. and Shyy, W., Computations of drop dynamics with the immersed boundary method, part 1: numerical algorithm and buoyancy-induced effect, Numerical Heat Transfer: Part B: Fundamentals, vol. **44**, no. 2, pp. 101–118, 2003.
66. Francois, M. and Shyy, W., Computations of drop dynamics with the immersed boundary method, part 2: Drop impact and heat transfer, Numerical heat transfer: part B: fundamentals, vol. **44**, no. 2, pp. 119–143, 2003.
67. Bejan, A., Convection heat transfer, John wiley & sons, 2013.
68. Bergman, T.L., Incropera, F.P., DeWitt, D.P., and Lavine, A.S., Fundamentals of heat and mass transfer, John Wiley & Sons, 2011.
69. Wang, Z., Fan, J., Luo, K., and Cen, K., Immersed boundary method for the simulation of flows with heat transfer, International Journal of Heat and Mass Transfer, vol. **52**, no. 19-20, pp. 4510–4518, 2009.
70. Ren, W., Shu, C., Wu, J., and Yang, W., Boundary condition-enforced immersed boundary method for thermal flow problems with Dirichlet temperature condition and its applications, Computers & Fluids, vol. **57**, pp. 40–51, 2012.
71. Kalyana Raman, S., Arul Prakash, K., and Vengadesan, S., Natural convection from a heated elliptic cylinder with a different axis ratio in a square enclosure, Numerical Heat Transfer, Part A: Applications, vol. **62**, no. 8, pp. 639–658, 2012.

72. Paul, I., Arul Prakash, K., and Vengadesan, S., Forced convective heat transfer from unconfined isothermal and isoflux elliptic cylinders, Numerical Heat Transfer, Part A: Applications, vol. **64**, no. 8, pp. 648–675, 2013.
73. Shu, C., Ren, W., and Yang, W., Novel immersed boundary methods for thermal flow problems, International Journal of Numerical Methods for Heat & Fluid Flow, 2013.
74. Tavassoli, H., Kriebitzsch, S., Van der Hoef, M., Peters, E., and Kuipers, J., Direct numerical simulation of particulate flow with heat transfer, International Journal of Multiphase Flow, vol. **57**, pp. 29–37, 2013.
75. Santarelli, C., Kempe, T., and Fröhlich, J., Immersed boundary methods for heat transfer, International Journal of Numerical Methods for Heat & Fluid Flow, 2016.
76. Lai, M.C. and Peskin, C.S., An immersed boundary method with formal second-order accuracy and reduced numerical viscosity, Journal of computational Physics, vol. **160**, no. 2, pp. 705–719, 2000.
77. Su, S.W., Lai, M.C., and Lin, C.A., An immersed boundary technique for simulating complex flows with rigid boundary, Computers & fluids, vol. **36**, no. 2, pp. 313–324, 2007.
78. Shin, S.J., Huang, W.X., and Sung, H.J., Assessment of regularized delta functions and feedback forcing schemes for an immersed boundary method, International Journal for Numerical Methods in Fluids, vol. **58**, no. 3, pp. 263–286, 2008.
79. Zhang, N., Zheng, Z., and Eckels, S., Study of heat-transfer on the surface of a circular cylinder in flow using an immersed-boundary method, International Journal of Heat and Fluid Flow, vol. **29**, no. 6, pp. 1558–1566, 2008.
80. Saiki, E. and Biringen, S., Numerical simulation of a cylinder in uniform flow: application of a virtual boundary method, Journal of computational physics, vol. **123**, no. 2, pp. 450–465, 1996.
81. Tajiri, K., Nishida, H., and Tanaka, M., Numerical simulation of incompressible flows with heat transfer using seamless immersed boundary method, Journal of Computational Science and Technology, vol. **7**, no. 2, pp. 286–296, 2013.
82. Xia, J., Luo, K., and Fan, J., A ghost-cell based high-order immersed boundary method for inter-phase heat transfer simulation, International Journal of Heat and Mass Transfer, vol. **75**, pp. 302–312, 2014.
83. Kumar, M. and Natarajan, G., Diffuse-interface immersed-boundary framework for conjugate-heat-transfer problems, Physical Review E, vol. **99**, no. 5, p. 053304, 2019.
84. Favre, F., Antepara, O., Oliet, C., Lehmkuhl, O., and Perez-Segarra, C.D., An immersed boundary method to conjugate heat transfer problems in complex geometries. Application to an automotive antenna, Applied Thermal Engineering, vol. **148**, pp. 907–928, 2019.
85. Kim, J., Kim, D., and Choi, H., An immersed-boundary finite-volume method for simulations of flow in complex geometries, Journal of computational physics, vol. **171**, no. 1, pp. 132–150, 2001.
86. Pan, D., A simple and accurate ghost cell method for the computation of incompressible flows over immersed bodies with heat transfer, Numerical Heat Transfer, Part B: Fundamentals, vol. **58**, no. 1, pp. 17–39, 2010.
87. Pan, D., A general boundary condition treatment in immersed boundary methods for incompressible Navier-Stokes equations with heat transfer, Numerical Heat Transfer, Part B: Fundamentals, vol. **61**, no. 4, pp. 279–297, 2012.

88. Luo, K., Zhuang, Z., Fan, J., and Haugen, N.E.L., A ghost-cell immersed boundary method for simulations of heat transfer in compressible flows under different boundary conditions, International Journal of Heat and Mass Transfer, vol. **92**, pp. 708–717, 2016.

89. Luo, K., Mao, C., Zhuang, Z., Fan, J., and Haugen, N.E.L., A ghost-cell immersed boundary method for the simulations of heat transfer in compressible flows under different boundary conditions Part-II: Complex geometries, International Journal of Heat and Mass Transfer, vol. **104**, pp. 98–111, 2017.

90. Seo, J.H. and Mittal, R., A high-order immersed boundary method for acoustic wave scattering and low-Mach number flow-induced sound in complex geometries, Journal of computational physics, vol. **230**, no. 4, pp. 1000–1019, 2011.

91. Xia, J., Luo, K., and Fan, J., Simulating heat transfer from moving rigid bodies using high-order ghost-cell based immersed-boundary method, International Journal of Heat and Mass Transfer, vol. **89**, pp. 856–865, 2015.

92. Pacheco-Vega, A., Pacheco, J.R., and Rodić, T., A general scheme for the boundary conditions in convective and diffusive heat transfer with immersed boundary methods, 2007.

93. Nagendra, K., Tafti, D.K., and Viswanath, K., A new approach for conjugate heat transfer problems using immersed boundary method for curvilinear grid based solvers, Journal of Computational Physics, vol. **267**, pp. 225–246, 2014.

94. Iaccarino, G. and Moreau, S., Natural and forced conjugate heat transfer in complex geometries on cartesian adapted grids, Journal of Fluids Engineering, vol. **128**, no. 4, pp. 838–846, 2006.

95. Kang, S., Iaccarino, G., and Ham, F., DNS of buoyancy-dominated turbulent flows on a bluff body using the immersed boundary method, Journal of Computational Physics, vol. **228**, no. 9, pp. 3189–3208, 2009.

96. Oh, T.K., Tafti, D.K., and Nagendra, K., Fully Coupled Large Eddy Simulation-Conjugate Heat Transfer Analysis of a Ribbed Cooling Passage Using the Immersed Boundary Method, Journal of Turbomachinery, vol. **143**, no. 4, p. 041012, 2021.

97. de Marinis, D., de Tullio, M.D., Napolitano, M., and Pascazio, G., Improving a conjugate-heat-transfer immersed-boundary method, International Journal of Numerical Methods for Heat & Fluid Flow, vol. **26**, no. 3/4, pp. 1272–1288, 2016.

98. Monge, A. and Birken, P., On the convergence rate of the Dirichlet–Neumann iteration for unsteady thermal fluid–structure interaction, Computational Mechanics, vol. **62**, no. 3, pp. 525–541, 2018.

99. Chand, K., Sharma, M., and De, A.K., Significance of near-wall dynamics in enhancement of heat flux for roughness aided turbulent Rayleigh–Bénard convection, Physics of Fluids, vol. **33**, no. 6, p. 065114, 2021.

100. Kim, J. and Choi, H., An immersed-boundary finite-volume method for simulation of heat transfer in complex geometries, KSME international journal, vol. **18**, no. 6, pp. 1026–1035, 2004.

101. Pacheco, J., Pacheco-Vega, A., Rodić, T., and Peck, R., Numerical simulations of heat transfer and fluid flow problems using an immersed-boundary finite-volume method on nonstaggered grids, Numerical Heat Transfer, Part B: Fundamentals, vol. **48**, no. 1, pp. 1–24, 2005.

102. Shinn, A., Goodwin, M., and Vanka, S., Immersed boundary computations of shear-and

buoyancy-driven flows in complex enclosures, International Journal of Heat and Mass Transfer, vol. **52**, no. 17-18, pp. 4082–4089, 2009.

103. Mark, A., Svenning, E., and Edelvik, F., An immersed boundary method for simulation of flow with heat transfer, International Journal of Heat and Mass Transfer, vol. **56**, pp. 424–435, 2013.
104. Ashrafizadeh, A. and Hosseinjani, A.A., A phenomenological study on the convection heat transfer around two enclosed rotating cylinders via an immersed boundary method, International Journal of Heat and Mass Transfer, vol. **107**, pp. 667–685, 2017.
105. Ji, C., Munjiza, A., and Williams, J., A novel iterative direct-forcing immersed boundary method and its finite volume applications, Journal of Computational Physics, vol. **231**, no. 4, pp. 1797–1821, 2012.
106. Garg, H., Soti, A.K., and Bhardwaj, R., A sharp interface immersed boundary method for vortex-induced vibration in the presence of thermal buoyancy, Physics of Fluids, vol. **30**, no. 2, p. 023603, 2018.
107. Das, S., Panda, A., Deen, N., and Kuipers, J., A sharp-interface immersed boundary method to simulate convective and conjugate heat transfer through highly complex periodic porous structures, Chemical Engineering Science, vol. **191**, pp. 1–18, 2018.
108. Łapka, P. and Furmański, P., Immersed Boundary Method for Radiative Heat Transfer Problems in Nongray Media With Complex Internal and External Boundaries, Journal of Heat Transfer, vol. **139**, no. 2, 2017.
109. Kedia, K.S., Safta, C., Ray, J., Najm, H.N., and Ghoniem, A.F., A second-order coupled immersed boundary-SAMR construction for chemically reacting flow over a heat-conducting Cartesian grid-conforming solid, Journal of Computational Physics, vol. **272**, pp. 408–428, 2014.
110. Soti, A.K., Bhardwaj, R., and Sheridan, J., Flow-induced deformation of a flexible thin structure as manifestation of heat transfer enhancement, International Journal of Heat and Mass Transfer, vol. **84**, pp. 1070–1081, 2015.
111. Kumar, V., Garg, H., Sharma, G., and Bhardwaj, R., Harnessing flow-induced vibration of a D-section cylinder for convective heat transfer augmentation in laminar channel flow, Physics of Fluids, vol. **32**, no. 8, p. 083603, 2020.
112. Wright, P., Why do elephants flap their ears?, African Zoology, vol. **19**, no. 4, pp. 266–269, 1984.
113. Koffi, M., Jiji, L., and Andreopoulos, Y., Why do elephants flap their ears?, In APS Division of Fluid Dynamics Meeting Abstracts, Vol. 62, pp. AE–009, 2009.
114. Bhardwaj, R. and Mittal, R., Benchmarking a coupled immersed-boundary-finite-element solver for large-scale flow-induced deformation, AIAA journal, vol. **50**, pp. 1638–1642, 2012.
115. Mittal, R., Zheng, X., Bhardwaj, R., Seo, J.H., Xue, Q., and Bielamowicz, S., Toward a simulation-based tool for the treatment of vocal fold paralysis, Frontiers in physiology, vol. **2**, p. 19, 2011.
116. Mishra, R., Kulkarni, S.S., Bhardwaj, R., and Thompson, M.C., Response of a linear viscoelastic splitter plate attached to a cylinder in laminar flow, Journal of Fluids and Structures, vol. **87**, pp. 284–301, 2019.

117. Griffith, M.D. and Leontini, J.S., Sharp interface immersed boundary methods and their application to vortex-induced vibration of a cylinder, Journal of Fluids and Structures, vol. **72**, pp. 38–58, 2017.

118. Williamson, C.H. and Govardhan, R., Vortex-induced vibrations, Annu. Rev. Fluid Mech., vol. **36**, pp. 413–455, 2004.

119. Bungartz, H.J. and Schäfer, M., Fluid-structure interaction: modelling, simulation, optimisation, Springer-Verlag, 2006.

120. Turek, S. and Hron, J., Proposal for numerical benchmarking of fluid-structure interaction between an elastic object and laminar incompressible flow, Lecture Notes in Computational Science and Engineering, vol. **53**, p. 371, 2006.

121. Donea, J., Huerta, A., Ponthot, J.P., and Rodríguez-Ferran, A., Arbitrary Lagrangian–Eulerian Methods, Encyclopedia of computational mechanics, 2004.

122. Souli, M. and Benson, D.J., Arbitrary Lagrangian Eulerian and fluid-structure interaction: numerical simulation, John Wiley & Sons, 2013.

123. Heil, M., Hazel, A.L., and Boyle, J., Solvers for large-displacement fluid–structure interaction problems: segregated versus monolithic approaches, Computational Mechanics, vol. **43**, no. 1, pp. 91–101, 2008.

124. Ryzhakov, P., Rossi, R., Idelsohn, S., and Onate, E., A monolithic Lagrangian approach for fluid–structure interaction problems, Computational mechanics, vol. **46**, no. 6, pp. 883–899, 2010.

125. van Brummelen, E.H., Added mass effects of compressible and incompressible flows in fluid-structure interaction, ASME Journal of Applied Mechanics, vol. **76(2)**, p. 021206, 2009.

126. Zheng, X., Xue, Q., Mittal, R., and Beilamowicz, S., A coupled sharp–interface immersed boundary–finite–element method for flow–structure interaction with application to human phonation, Journal of biomechanical engineering, vol. **132**, no. 11, p. 111003, 2010.

127. Küttler, U. and Wall, W.A., Fixed-point fluid–structure interaction solvers with dynamic relaxation, Computational mechanics, vol. **43**, no. 1, pp. 61–72, 2008.

128. Borazjani, I., Ge, L., and Sotiropoulos, F., Curvilinear immersed boundary method for simulating fluid structure interaction with complex 3D rigid bodies, Journal of Computational physics, vol. **227**, no. 16, pp. 7587–7620, 2008.

129. Kim, W., Lee, I., and Choi, H., A weak-coupling immersed boundary method for fluid–structure interaction with low density ratio of solid to fluid, Journal of Computational Physics, vol. **359**, pp. 296–311, 2018.

130. Kundu, A., Soti, A.K., Garg, H., Bhardwaj, R., and Thompson, M.C., Computational modeling and analysis of flow-induced vibration of an elastic splitter plate using a sharp-interface immersed boundary method, SN Applied Sciences, vol. **2**, pp. 1–23, 2020.

131. Tahoe is an open source C++ finite element solver, which was developed at Sandia National Labs, CA. (http://sourceforge.net/projects/tahoe/).

132. Tian, F.B., Dai, H., Luo, H., Doyle, J.F., and Rousseau, B., Fluid–structure interaction involving large deformations: 3D simulations and applications to biological systems, Journal of computational physics, vol. **258**, pp. 451–469, 2014.

133. Goza, A. and Colonius, T., A strongly-coupled immersed-boundary formulation for thin elastic structures, Journal of Computational Physics, vol. **336**, pp. 401–411, 2017.

134. Thekkethil, N. and Sharma, A., Level set function–based immersed interface method and benchmark solutions for fluid flexible-structure interaction, International Journal for Numerical Methods in Fluids, vol. **91**, no. 3, pp. 134–157, 2019.

135. Kumar, M. and Roy, S., Immersed boundary method simulation of natural convection over fixed and oscillating cylinders in square enclosure, International Journal of Heat and Fluid Flow, vol. **61**, pp. 407–424, 2016.

136. Feng, Z.G. and Michaelides, E.E., Proteus: a direct forcing method in the simulations of particulate flows, Journal of Computational Physics, vol. **202**, no. 1, pp. 20–51, 2005.

137. Feng, Z.G. and Musong, S.G., Direct numerical simulation of heat and mass transfer of spheres in a fluidized bed, Powder technology, vol. **262**, pp. 62–70, 2014.

138. Musong, S.G., Feng, Z.G., Michaelides, E.E., and Mao, S., Application of a three-dimensional immersed boundary method for free convection from single spheres and aggregates, Journal of Fluids Engineering, vol. **138**, no. 4, 2016.

139. Menon, K. and Mittal, R., On the initiation and sustenance of flow-induced vibration of cylinders: insights from force partitioning, Journal of Fluid Mechanics, vol. **907**, 2021.

140. Blevins, R.D., Flow-induced vibration, New York, 1977.

141. Naudascher, E. and Rockwell, D., Flow-induced vibrations: an engineering guide, Routledge, 2017.

142. Païdoussis, M.P., Price, S.J., and De Langre, E., Fluid-structure interactions: cross-flow-induced instabilities, Cambridge University Press, 2010.

143. Garg, H., Soti, A.K., and Bhardwaj, R., Vortex-induced vibration of a cooled circular cylinder, Physics of Fluids, vol. **31**, no. 8, p. 083608, 2019.

144. Garg, H., Soti, A.K., and Bhardwaj, R., Vortex-induced vibration and galloping of a circular cylinder in presence of cross-flow thermal buoyancy, Physics of Fluids, vol. **31**, no. 11, p. 113603, 2019.

145. Garg, H., Soti, A.K., and Bhardwaj, R., Thermal buoyancy induced suppression of wake-induced vibration, International Communications in Heat and Mass Transfer, vol. **118**, p. 104790, 2020.

146. Park, S.G., Kim, B., Chang, C.B., Ryu, J., and Sung, H.J., Enhancement of heat transfer by a self-oscillating inverted flag in a Poiseuille channel flow, International Journal of Heat and Mass Transfer, vol. **96**, pp. 362–370, 2016.

147. Lee, J.B., Park, S.G., Kim, B., Ryu, J., and Sung, H.J., Heat transfer enhancement by flexible flags clamped vertically in a Poiseuille channel flow, international journal of heat and mass transfer, vol. **107**, pp. 391–402, 2017.

148. Lee, J.B., Park, S.G., and Sung, H.J., Heat transfer enhancement by asymmetrically clamped flexible flags in a channel flow, international journal of heat and mass transfer, vol. **116**, pp. 1003–1015, 2018.

149. Rips, A., Shoele, K., and Mittal, R., Heat transfer enhancement in laminar flow heat exchangers due to flapping flags, Physics of Fluids, vol. **32**, no. 6, p. 063603, 2020.

150. Rips, A. and Mittal, R., Flutter-enhanced mixing in small-scale mixers, Physics of Fluids, vol. **31**, no. 10, p. 107107, 2019.

151. Rips, A. and Mittal, R., Enhanced mixing at inertial microscales using flow-induced flutter, Physical Review Fluids, vol. **4**, no. 5, p. 054501, 2019.

152. Rubinsky, B., Cryosurgery, Annual review of biomedical engineering, vol. **2**, no. 1, pp. 157–187, 2000.

153. Roemer, R.B., Engineering aspects of hyperthermia therapy, Annual Review of Biomedical Engineering, vol. **1**, no. 1, pp. 347–376, 1999.

154. Berjano, E.J., Theoretical modeling for radiofrequency ablation: state-of-the-art and challenges for the future, Biomedical engineering online, vol. **5**, no. 1, pp. 1–17, 2006.

155. Pennes, H.H., Analysis of tissue and arterial blood temperatures in the resting human forearm, Journal of applied physiology, vol. **1**, no. 2, pp. 93–122, 1948.

156. Ge, M., Chua, K., Shu, C., and Yang, W., Analytical and numerical study of tissue cryofreezing via the immersed boundary method, International Journal of Heat and Mass Transfer, vol. **83**, pp. 1–10, 2015.

157. Ge, M., Shu, C., Chua, K., and Yang, W., Numerical analysis of a clinically-extracted vascular tissue during cryo-freezing using immersed boundary method, International Journal of Thermal Sciences, vol. **110**, pp. 109–118, 2016.

158. Shao, Y., Arjun, B., Leo, H., and Chua, K., A computational theoretical model for radiofrequency ablation of tumor with complex vascularization, Computers in biology and medicine, vol. **89**, pp. 282–292, 2017.

159. Bertin, J.J., Hypersonic aerothermodynamics, AIAA, 1994.

160. Sundén, B. and Fu, J., Heat Transfer in Aerospace Applications, Academic Press, 2016.

161. De Palma, P., De Tullio, M., Pascazio, G., and Napolitano, M., An immersed-boundary method for compressible viscous flows, Computers & fluids, vol. **35**, no. 7, pp. 693–702, 2006.

162. Bailoor, S., Annangi, A., Seo, J.H., and Bhardwaj, R., Fluid–structure interaction solver for compressible flows with applications to blast loading on thin elastic structures, Applied Mathematical Modelling, vol. **52**, pp. 470–492, 2017.

163. Wang, L., Currao, G.M., Han, F., Neely, A.J., Young, J., and Tian, F.B., An immersed boundary method for fluid–structure interaction with compressible multiphase flows, Journal of computational physics, vol. **346**, pp. 131–151, 2017.

164. Bhardwaj, R., Ziegler, K., Seo, J.H., Ramesh, K., and Nguyen, T.D., A computational model of blast loading on the human eye, Biomechanics and modeling in mechanobiology, vol. **13**, no. 1, pp. 123–140, 2014.

165. Bailoor, S., Bhardwaj, R., and Nguyen, T.D., Effectiveness of eye armor during blast loading, Biomechanics and modeling in mechanobiology, vol. **14**, no. 6, pp. 1227–1237, 2015.

166. Chaudhuri, A., Hadjadj, A., and Chinnayya, A., On the use of immersed boundary methods for shock/obstacle interactions, Journal of Computational Physics, vol. **230**, no. 5, pp. 1731–1748, 2011.

167. Kumar, V., Sharma, A., and Singh, R., Central upwind scheme based immersed boundary method for compressible flows around complex geometries, Computers & Fluids, vol. **196**, p. 104349, 2020.

168. Greene, P.T., Eldredge, J.D., Zhong, X., and Kim, J., A high-order multi-zone cut-stencil method for numerical simulations of high-speed flows over complex geometries, Journal of Computational Physics, vol. **316**, pp. 652–681, 2016.

169. Greene, P., Eldredge, J., Zhong, X., and Kim, J., Numerical study of hypersonic flow over an isolated roughness with a high-order cut-cell method, In 41st AIAA Fluid Dynamics Conference and Exhibit, p. 3249, 2011.

170. Duan, L., Wang, X., and Zhong, X., A high-order cut-cell method for numerical simulation of hypersonic boundary-layer instability with surface roughness, Journal of computational physics, vol. **229**, no. 19, pp. 7207–7237, 2010.

171. Bridel-Bertomeu, T., Immersed boundary conditions for hypersonic flows using ENO-like least-square reconstruction, Computers & Fluids, vol. **215**, p. 104794, 2021.

172. Ollivier-Gooch, C.F., Quasi-ENO schemes for unstructured meshes based on unlimited data-dependent least-squares reconstruction, Journal of Computational Physics, vol. **133**, no. 1, pp. 6–17, 1997.

173. Brahmachary, S., Natarajan, G., Kulkarni, V., Sahoo, N., Ashok, V., and Kumar, V., Role of solution reconstruction in hypersonic viscous computations using a sharp interface immersed boundary method, Physical Review E, vol. **103**, no. 4, p. 043302, 2021.